25/1076

NUREG/CR-1076

# Development of High-Sensitivity Ultrasonic Techniques for In-Service Inspection of Nuclear Reactors

Annual Report
October 1977 - September 1978

Prepared by M. Linzer, S. I. Parks, D. R. Dietz, S. J. Norton

National Bureau of Standards

Prepared for
U. S. Nuclear Regulatory
Commission

NEWARK PUBLIC LIBRARY
DEC. 5 1979
U. S. GOVT. PUBS.
DEPOSITORY 376

Y 3.N 88:

NOTICE

This report was prepared as an account of work sponsored by an agency of the United States Government. Neither the United States Government nor any agency thereof, or any of their employees, makes any warranty, expressed or implied, or assumes any legal liability or responsibility for any third party's use, or the results of such use, of any information, apparatus product or process disclosed in this report, or represents that its use by such third party would not infringe privately owned rights.

Available from

GPO Sales Program
Division of Technical Information and Document Control
U. S. Nuclear Regulatory Commission
Washington, D. C. 20555

and

National Technical Information Service
Springfield, Virginia 22161

NUREG/CR-1076

# Development of High-Sensitivity Ultrasonic Techniques for In-Service Inspection of Nuclear Reactors

Annual Report
October 1977 - September 1978

Manuscript Completed: June 1979
Date Published: November 1979

Prepared by
M. Linzer, S. I. Parks, D. R. Dietz, S. J. Norton

Center for Materials Science
National Measurement Laboratory
National Bureau of Standards
Washington, D.C. 20234

Prepared for
Division of Reactor Safety Research
Office of Nuclear Regulatory Research
U.S. Nuclear Regulatory Commission
Washington, D.C. 20555
NRC FIN No. B5680

ABSTRACT

During the period covered by this report, the expanding-aperture annular array system and an analysis of the focusing properties of an annular array were completed. Experiments were also undertaken to test the efficacy of spatial-temporal averaging to improve the signal-to-grain noise ratio in austenitic steel.

TABLE OF CONTENTS


| | PAGE |
|---|---|
| I. Introduction | 1 |
| II. Wideband Annular Array Response | 1 |
| 1. Introduction | 1 |
| 2. Wideband Response | 3 |
| 3. Calculated Response of a Wideband Lens | 8 |
| 4. Comparison of Calculated and Experimental Results | 10 |
| 5. Conclusion | 13 |
| III. Expanding-Aperture Annular Array | 14 |
| 1. Introduction | 14 |
| 2. Annular Array Design Considerations | 16 |
| 3. System Design | 24 |
| 4. Resolution Measurements | 28 |
| 5. Conclusions | 32 |
| IV. Spatial-Temporal Averaging | 41 |
| 1. Spatial-Temporal Averaging from Extended Flaws | 42 |
| 2. Spatial-Temporal Averaging from Small Flaws | 45 |
| 3. Summary | 47 |


TABLE


| | |
|---|---|
| Table 1. Summary of Spatial-temporal Averaging Experiments | 46 |


FIGURES

Section II. Wideband Annular Array Response


| | |
|---|---|
| Fig. 1. (a) Impulse response in focal plane of a circular lens. (b) Extent of impulse response in time as a function of off-axis distance ρ | 5 |
| Fig. 2. Aperture weighting functions for the circular lens | 8 |
| Fig. 3. Calculated focal plane response of the circular lens with approximately 11 percent bandwidth | 9 |
| Fig. 4. Calculated focal plane response of the circular lens with 50 percent bandwidth | 10 |
| Fig. 5. Calculated focal plane response of the circular lens with 100 percent bandwidth | 10 |
| Fig. 6. Measured pulse shape and its spectrum | 11 |




READEX FICHE best copy available

Fig. 7. Field pattern at 10 cm generated by a 0.4 cm diameter piston transmitter and a thin, 1.4 diameter annulus, receiver. The solid line is the calculated response and the dashed line is the measured response. . . . . 11

Fig. 8. Calculated response of the ten element, 3.2 cm o.d., annular array focused at 10 cm on transmit and receive. . . 12

Fig. 9. Measured response of the ten element annular array focused at 10 cm on transmit and receive. . . . . 12

Section III. Expanding-Aperture Annular Array

Fig. 1. Envelope of the focal plane response of a circular lens (top) and a thin annulus of one-half the lens diameter (bottom). . . . . 16

Fig. 2. Beam profiles for an annulus driven with a pulse of 40% bandwidth (top), and a single frequency waveform (bottom). The annulus has a radius of 11 mm and a width of 0.6 mm . . . . . 17

Fig. 3. Diagram of an annulus showing the path differences between the inner and outer edges with respect to a point on axis . . . . . 20

Fig. 4. Operation of the expanding-aperture array with dynamic focusing on receive . . . . . 22

Fig. 5. Time delay relative to the central element required for each annulus as a function of focal length. . . . . 25

Fig. 6. Block diagram of the receiver amplifiers and analog multiplexer of the dynamically-focused array. . . . . 26

Fig. 7. Schematic diagram of the cascode amplifier-multiplexer circuit. Transistors Si are used as analog switches toggled by the logic decoder. . . . . 27

Fig. 8. Schematic diagram of the circuit used to generate a variable focus on transmit. . . . . 27

Fig. 9. Beam profiles for the annular array focused on both transmit and receive at 3 and 15 cm . . . . . 29

Fig. 10. Beam profiles for the annular array, focused on receive, comparing the use of a point or line focus on transmit. . . 29

Fig. 11. Beam profiles for the annular array comparing the results of log processing before and after coherent summation. A point focus was generated on transmit . . . . 30

Fig. 12. Beam profiles for the array focused to a point on transmit with a 2.2 diameter annulus used as the receiver. . . . . 30

Fig. 13. Summary of resolution measurements with the focused annular array . . . . . 31

Fig. 14. B-scans of AIUM test object with a single, fixed-focus transducer (left) and with the dynamically-focused annular array (right) . . . . . 32

Fig. 15. High voltage pulser . . . . . 34

Fig. 16. Preamplifier. . . . . 35

Fig. 17. Log/linear amplifier. . . . . 36

Fig. 18. Block diagram of digital control for the fast analog multiplexer . . . . . 37

Fig. 19. Address counter and memory. . . . . 38

Fig. 20. Decoder and switch-driver circuit . . . . . 39

Section IV. Spatial-Temporal Averaging

Fig. 1. Specimen configuration for spatial-temporal averaging of signals from extended flaws. . . . . 43

Fig. 2. Schematic diagram of transmitter-receiver probes . . . . . 43

Figs. 3-5. Single (a) and averaged (b) A-scan signals showing reflections from 3 mm diameter side-drilled holes at depths of 38 mm (Fig. 3), 27 mm (Fig. 4), and 25 mm (Fig. 5). . . . . 44

Fig. 6. Single (a) and averaged (b) A-scans showing reflections from backwall of austenitic steel block. . . . . 45

Fig. 7. Single (a) and averaged (b) A-scan signals in region of 1 mm flat bottom hole. . . . . 47

# I. INTRODUCTION

Our program in FY78 had three principal objectives:

1. Complete analysis of the annular array, in both the narrow band and wide band cases, and compare with experimental beam plots.

2. Complete manuscript and documentation on the expanding-aperture annular array design.

3. Apply the high-speed signal averager to spatial-temporal averaging of grain scattering in austenitic stainless steel.

These objectives have all been met. In Section II, a paper on wideband annular array analysis, published in the 1978 IEEE Ultrasonics Symposium Proceedings, pp. 206-211, is reprinted. In Section III, a paper on the expanding-aperture array, which appears in slightly modified form in Ultrasonic Imaging, 1, 56-75 (1979) is presented. Also included is an Appendix on additional circuit documentation to serve as a guide for those wishing to build a dynamic-focusing system based on our design. Finally, in Section IV, the results of experiments on spatial-temporal averaging carried out in collaboration with Dr. H. Wustenberg of BAM (Berlin, W. Germany) and Drs. K. Goebells and W. Mohr of the Institut für Zerstorungsfreie Prufverfahren (Saarbrucken, W. Germany) are presented.

# II. WIDEBAND ANNULAR ARRAY RESPONSE

Theoretical calculations and experimental measurements of the response of a wideband annular array are presented. An analytical model of the impulse response of both a circular lens and thin annulus is described. The wideband response is then calculated by convolving the impulse response with the driving function. This formalism is extended to describe the focal plane response of an annular array pulse echo imaging system. The transducer transfer function is incorporated into the description of the system response. A method is described for measuring this transfer function and using it in calculations of the focal plane response. For the circular aperture, theoretical results are presented showing the effects of bandwidth and apodization on beam width and sidelobe level. For the annular array, comparisons are made between the calculated field patterns, using the system transfer function, and measured results.

## 1. Introduction

The quality of an image obtained with an ultrasound array depends upon the resolution and dynamic range of the imaging system. The azimuthal

(lateral) resolution is proportional to the width of the mainlobe and the useful dynamic range is limited by the height of the sidelobes. The beam width and sidelobe levels are determined by array geometry, the number of array elements, and the system bandwidth. Since the complexity of an array system increases with the number of array elements, efficient design procedures are required for optimizing image quality with a finite number of elements. The first step in this process is the development of analytical models for accurately calculating array response.

Extensive work has been done in narrow bandwidth design of both one and two dimensional arrays. In the theory of linear arrays with uniform element spacing, optimization techniques have been developed for minimizing the mainlobe width for a given sidelobe level. An example is the Dolph-Chebyshev array [1,2]. The optimization technique of Dolph has also been generalized to the circular aperture problem [3].

These models relate the mainlobe width and sidelobe level to amplitude weighting of the aperture and form the basis for the design of sparse arrays. There is some equivalence between the effects of amplitude weighting of the array elements and the density of equally weighted elements in determining the width of the main lobe and the height of the low order sidelobes. It is difficult, however, to control the height of the higher order sidelobes with a sparse, narrow bandwidth array.

In contrast to electromagnetic arrays, which operate essentially in a c.w. mode, ultrasound arrays employ large bandwidths. Bandwidths of 50 percent and greater are practical. The short pulses generated by wideband transducers improve the temporal (range) resolution of pulse-echo imaging systems and have a very significant effect on the azimuthal field patterns. The efficient design of ultrasound arrays requires an understanding of the effects of system bandwidth on the azimuthal field pattern.

Some work on wideband array design has been reported. The impulse response of an array has been calculated and applied to the problem of Doppler radars [4]. Miller and Thurstone [5] have described a model of a short-pulse linear array used in ultrasound imaging. Stepanishen [6] has calculated the near and far field transient response of a baffled piston of arbitrary shape. An analysis of the wideband imaging problem has been carried out by Norton and Macovski [7] and serves as the basis for this work.

An exact solution of the wideband imaging problem would require an analysis in four dimensions, three spatial dimensions and the temporal dimension. In the approach taken in reference 7 and followed here, the problem is simplified by considering only the temporal response of the field in the focal plane of the aperture. This approach is particularly appropriate for modeling the response of dynamically-focused arrays. With dynamic focusing, the focal plane of the receiver moves through the medium with the transmitted pulse. Thus an analysis of the focal plane response of a wideband array should provide a reasonable approximation of the point spread function of the imaging system. In this paper, we present theoretical calculations and experimental measurements of the response of an annular array excited by a short pulse.

In the following section, we briefly discuss the analytical model used for calculating the wideband response of a circular aperture and show how the transfer function of the source enters into the description of the field which is generated. We then model a pulse echo experiment employing elements from an annular array and show how the required transfer functions of the transmitter and receiver can be determined. Using this formalism, we present in Section 3 computer models of the focal plane response of a circular aperture for several bandwidths and apodizations. In Section 4, experimentally measured beam patterns obtained with an annular array are compared with the calculated response based upon the model outlined in Section 2.

## 2. Wideband Response

We first outline the formalism for calculating the focal plane response of a circular lens driven by a wideband pulse. This formalism is applied to some specific examples in Section 3. We then describe the impulse response of a piston and a thin annulus. These results serve as the basis for the description of the pulse-echo response of a focused annular array.

The monochromatic focal plane response of a circularly symmetric aperture is given by [8]:

$$H(\rho,\bar{\nu}) = \frac{2\pi\bar{\nu}}{iz} e^{+i2\pi\bar{\nu}(z + \rho^2/2z)} \int_0^\infty A(r) J_o(2\frac{\pi r}{z}\rho\bar{\nu}) r dr \qquad (1)$$

where $\bar{\nu} \equiv 1/\lambda$, $\bar{t} \equiv ct$. Here, z is the focal length, $\rho$ is the off-axis distance in the focal plane, and A(r) is the circularly symmetric pupil

function. The integral is the Hankel transform, or the two dimensional Fourier transform, of the pupil function. These results are valid in the focal plane of the lens or in the far field of the aperture. The impulse response for this aperture can be found by taking the Fourier transform of $H(\rho,\bar{\nu})$:

$$h(\rho,\bar{t}) = \int_{-\infty}^{\infty} H(\rho,\bar{\nu})\, e^{-i2\pi\bar{\nu}\bar{t}}\, d\bar{\nu} \tag{2}$$

The response in the focal plane to an arbitrary driving function, $f(\bar{t})$, can then be calculated by convolving $f(\bar{t})$ with the impulse response:

$$p(\rho,\bar{t}) = f(\bar{t}) * h(\rho,\bar{t}) \tag{3}$$

For example, for a uniformly weighted circular aperture of radius R the pupil function is:

$$A(r) = \mathrm{circ}(r/R) \tag{4}$$

where $\mathrm{circ}(r/R) \equiv \begin{cases} 1 & r \leq R \\ 0 & r > R \end{cases}$.

The focal plane response is given by:

$$H_p(\rho,\bar{\nu}) = \frac{\bar{\nu}}{iz}\, e^{i2\pi\bar{\nu}(z + \rho^2/2z)}\, 2\pi R^2 \frac{J_1(2\pi R\rho\bar{\nu}/z)}{(2\pi R\rho\bar{\nu}/z)} \tag{5}$$

where $J_1(x)$ is the Bessel function of first order. The impulse response for this aperture is calculated in reference 7 and only the results are stated here:

$$h_p(\rho,\bar{t}) = \frac{1}{\pi\rho}\frac{d}{d\bar{t}_1}\left[\sqrt{R^2 - \left(\frac{z\bar{t}_1}{\rho}\right)^2}\ \mathrm{rect}\left(\frac{z\bar{t}_1}{2R\rho}\right)\right] \tag{6}$$

where $\bar{t}_1 \equiv \bar{t} - z - \rho^2/2z$ and $\mathrm{rect}(x) \equiv \begin{cases} 1 & |x| \leq 1/2 \\ 0 & |x| > 1/2 \end{cases}$.

At a point on the axis ($\rho = 0$):

$$h_p(0,\bar{t}) = \frac{R^2}{2z}\,\delta'(\bar{t} - z) \tag{7}$$

The impulse response of the uniformly weighted aperture is shown in Figure 1a. The shaded area in Figure 1b represents the extent of the impulse response in the time domain. The boundary of the shaded area corresponds to the time of arrival of energy from the edges of the focused aperture.

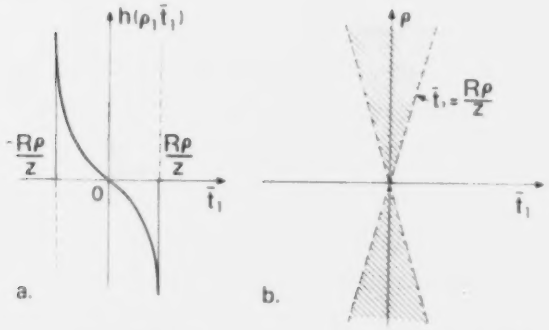


Fig. 1. (a) Impulse response in focal plane of a circular lens. (b) Extent of impulse response in time as a function of off-axis distance ρ.

In the frequency domain, $H_p(\rho,\bar{\nu})$ can be considered a low pass filter whose cutoff frequency decreases with the off-axis distance. In the time domain, the response in the focal plane to an arbitrary driving function $f(\bar{t})$ is then given by equation (3) which, for the uniformly weighted aperture, can be rewritten as:

$$p(\rho,t) = f'(\bar{t}) * \left[ \frac{1}{\pi\rho} \sqrt{R^2 - \left(\frac{z\bar{t}_1}{\rho}\right)^2}\ \mathrm{rect}\left(\frac{z\bar{t}_1}{2R\rho}\right) \right]. \qquad (8)$$

Here we have used the identity: $f(x)*g'(x)=f'(x)*g(x)$. The term in brackets is a weighted rectangle function whose width increases linearly with $\rho$. Thus, the response in the focal plane is the filtered time derivative of the driving function. At a point on the axis of the circular aperture, the time domain response is given by:

$$p(0,\bar{t}) = h_p(0,\bar{t}) * f(\bar{t}) = f(\bar{t}) * \frac{R^2}{2z}\ \delta'(\bar{t} - z) \qquad (9)$$

Likewise, it is easily shown that for a thin annulus, represented by a pupil function $A(r) = \delta(r-a)$, the impulse response in a plane parallel to the annulus, at a distance z, is given by:

$$h_a(\rho,\bar{t}) = \frac{1}{2\pi\rho} \frac{d}{dt_1} \left[ \frac{2a}{\sqrt{a^2 - \left(\frac{z\bar{t}_1}{\rho}\right)^2}}\ \mathrm{rect}\left(\frac{z\bar{t}_1}{2a\rho}\right) \right]. \qquad (10)$$

In the frequency domain,

$$H_a(\rho,\bar{\nu}) = \frac{\bar{\nu}}{iz} e^{+i2\pi\bar{\nu}(z + \rho^2/2z)} 2\pi a \, J_o(2\pi a\rho\bar{\nu}/z) \tag{11}$$

where $J_o$ is the zero order Bessel function. At a point on the axis:

$$h_a(0,\bar{t}) = \frac{a}{z}\delta'(\bar{t} - z) \tag{12}$$

In this model, the annulus is treated as a thin section of the focused lens and thus the quadratic time delay, corresponding to the path differences between different annuli and the focal point, has been compensated for.

So far we have described the field in the focal plane of an aperture driven by a wideband pulse. Next, we will extend the analysis to include the effects of the transmitter and receiver, and calculate the signal measured in a pulse echo experiment when a small target is present in the focal plane. An analysis of a pulse echo imaging system requires the transfer functions of both the transmitter and receiver. Given the problem of accurately modeling the transfer function of each array element and its associated electronics, it is desirable to present the problem in a manner such that the required transfer functions are easily measured. Here we outline the solution to this problem for the special case of the circularly symmetric elements of an annular array.

The annular array which we model consists of a central piston and several concentric annuli. The impulse response of the central element, a piston, and an annulus have been calculated in equations (6) and (10) respectively. We will assume that the plane of interest is in the far field of the array elements. This implies that there is no significant phase shift across the width of the annulus with respect to a point in the imaging plane. We will also assume that the array is focused by compensating for the quadratic time delay difference between elements.

We first describe the result of a pulse-echo measurement using the central element of the array as the transmitter and an annulus as the receiver. We will assume that the target is a small reflector with a flat frequency response over the bandwidth of interest. The off-axis distance, $\rho$, will now refer to the position of the target in the plane at a distance, $z$, from the array. In the frequency domain, the received voltage can be written:

$$V(\rho,\bar{\nu}) = F(\bar{\nu})\, H_p(\rho,\bar{\nu})\, G(\bar{\nu})\, H_a(\rho,\bar{\nu}) \ . \qquad (13)$$

$H_p(\rho,\bar{\nu})$ is the spatial factor for the piston of radius R, and $H_a(\rho,\bar{\nu})$ is the corresponding factor for the annulus, given in equations (5) and (10) respectively. $F(\bar{\nu})$ is the transfer function of the transmitting transducer mechanically loaded by the medium under investigation and electrically loaded by the source impedance. This is the transfer function that would be calculated in a one-dimensional transmission line model of the transducer with its mechanical and electrical terminations. $G(\bar{\nu})$ is the corresponding transfer function for the receiving transducer. If the transmitting transducer is driven by a voltage impulse, the standard technique for excitation, the received voltage as a function of time is:

$$v(\rho,\bar{t}) = f(\bar{t}) * h_p(\rho,\bar{t}) * g(t) * h_a(\rho,\bar{t}) \ . \qquad (14)$$

Using the results for $h_p(0,\bar{t})$ and $h_a(0,\bar{t})$ given earlier, we can calculate the received signal when the target is on the axis:

$$v(0,\bar{t}) = f(\bar{t}) * \frac{R^2}{2z}\,\delta'(\bar{t} - z) * g(\bar{t}) * \frac{a}{z}\,\delta'(\bar{t} - z)$$

$$= f'(\bar{t}) * g'(\bar{t}) * \frac{aR^2}{2z^2}\,\delta(\bar{t} - 2z) \ , \qquad (15)$$

or, in the frequency domain:

$$V(0,\bar{\nu}) \propto \nu^2\, F(\bar{\nu})\, G(\bar{\nu}) \ . \qquad (16)$$

Thus, the required transfer function, weighted by a factor $\bar{\nu}^2$, can be obtained with a single measurement on axis. The off-axis response in the frequency domain can then be calculated from equation 13, using the analytically derived expressions $H_p(\rho,\bar{\nu})$ (equation 5) and $H_a(\rho,\bar{\nu})$ (equation 11). The time domain response is found by taking the Fourier transform of equation (13).

The calculated response of the focused array is then simply a problem of superposition. For example, we can model the focal plane response for the case where the central piston of the array is used as the transmitter and the entire array is used as a focused receiver. In the frequency domain, the received voltage would be:

$$V(\rho,\bar{\nu}) = H_p(\rho,\bar{\nu}) F(\bar{\nu}) \left( \sum_{i=1}^{n} G_i(\bar{\nu}) H_{a_i}(\rho,\bar{\nu}) \right), \qquad (17)$$

where the sum is taken over all the array elements. The transfer functions $F(\bar{\nu})G_i(\bar{\nu})$ can be measured in the manner just described. If the array is focused on both transmit and receive, then the received signal would be:

$$V(\rho,\bar{\nu}) = \left(\sum_{i=1}^{n} H_{a_i}(\rho,\bar{\nu})F_i(\bar{\nu})\right)\left(\sum_{i=1}^{n} G_i(\bar{\nu})H_{a_i}(\rho,\bar{\nu})\right). \tag{18}$$

This model will be used in Section 4 to calculate the response of an annular array using its measured transfer function.

3. Calculated Response of a Wideband Lens

Equations (1) through (3) may be used to calculate the amplitude of the focal plane response of a circular aperture for different bandwidths and apodizations. These results provide insight into the effects of bandwidth on focal plane response and may be used in selecting the spacing of array elements in a sparse array.

The pupil functions employed are of the form:

$$A_m(r) = (R^2 - r^2)^m \operatorname{circ}(r/R) \tag{19}$$

for which the focal plane response in the frequency domain, $H_m(\rho,\bar{\nu})$, is proportional to the Lambda function of order $(m + 1)$. That is,

$$H_m(\rho,\bar{\nu}) \propto \Lambda_{m+1}\left(\frac{2\pi R\rho\bar{\nu}}{z}\right) \tag{20}$$

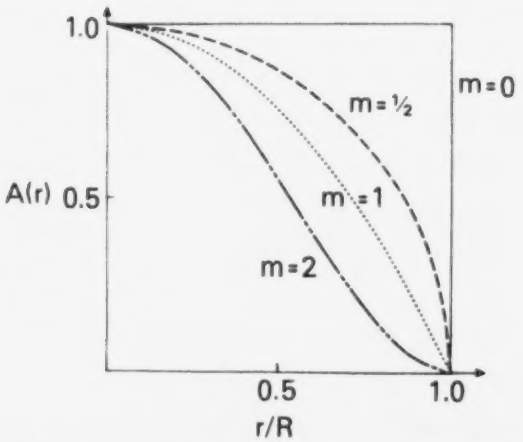


Fig. 2. Aperture weighting functions for the circular lens.

These apodizing functions are plotted in Figure 2 and the corresponding Lambda functions are tabulated below.[3]

$$\Lambda_1(x) \equiv \frac{J_1(x)}{x} \qquad \Lambda_2(x) \equiv \frac{8J_2(x)}{x^2}$$

$$\Lambda_{3/2}(x) \equiv \frac{3}{x^2}\left(\frac{\sin x}{x} - \cos x\right) \quad \Lambda_3(x) \equiv \frac{48J_3(x)}{x^3} \tag{21}$$

A model broadband pulse is used in this calculation and is of the form:

$$f(t) = e^{-(t/t_o)^2} \sin(2\pi f_o t) \ . \tag{22}$$

The bandwidth of the pulse will be defined here as $1/t_o$, and the percent bandwidth as $1/t_o f_o$.

In the frequency domain, the response in the focal plane is:

$$P(\rho,\bar{\nu}) = F(\bar{\nu})H_m(\rho,\bar{\nu}) \quad , \tag{23}$$

where $H_m(\rho,\bar{\nu})$ is proportional to the appropriate Lambda function and $F(\bar{\nu})$ is the Fourier transform of the pulse given in equation (22). Equation (23) is Fourier transformed to obtain the temporal response, $p(\rho,\bar{t})$, which is the amplitude of the acoustic field in the focal plane. To simulate a video detector which may be used to measure the field, $p(\rho,\bar{t})$ is rectified and then time-averaged over two periods of the pulse. This value is then plotted on a logarithmic scale in Figures 3 through 5.

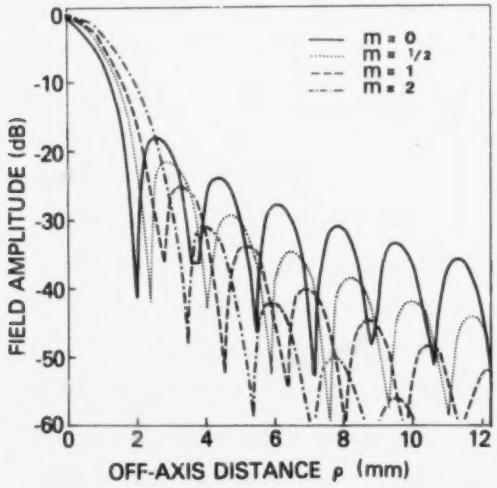


Fig. 3. Calculated focal plane response of the circular lens with approximately 11 percent bandwidth.

For the beam profiles shown in Figure 3, the bandwidth of the driving pulse was 11 percent. The solid curve, representing the response

of the uniformly weighted aperture, is approximately the absolute value of $H_p(\rho,\bar{\nu})$ in equation (5). The remaining curves are the resulting field patterns for the pupil functions, defined in equation (19), for values of m equal to 1/2, 1, and 2. For this relatively narrow bandwidth, they are approximately the absolute value of the Lambda functions of order (m + 1).

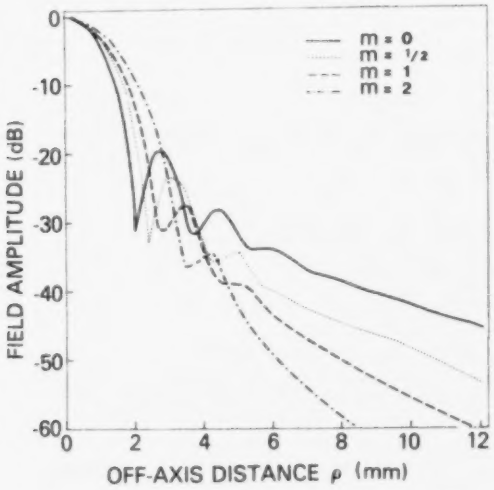


Fig. 4. Calculated focal plane response of the circular lens with 50 percent bandwidth.

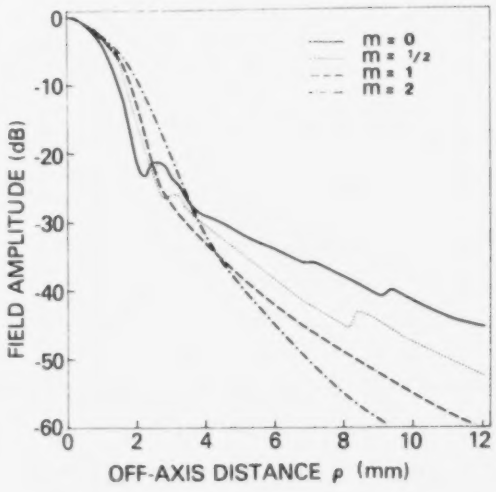


Fig. 5. Calculated focal plane response of the circular lens with 100 percent bandwidth.

In Figures 4 and 5, similar beam plots are shown for bandwidths of 50 percent and 100 percent. Note that while the amplitude of the sidelobes decrease as the bandwidth is increased, the -20 dB beam width is independent of bandwidth.

## 4. Comparisons of Calculated and Experimental Results

In this Section we will show examples of beam patterns calculated for a wideband annular array and compare them with experimental measurements.

The annular array used in these experiments was fabricated from a lead metaniobate plate resonant at 2.25 MHz which was back-loaded to provide an approximately 40 percent bandwidth. It has twelve elements with a maximum radius of 2 cm. The central element is a piston of radius 0.2 cm. The array system is described in detail in reference 9.

Measurements on the beam pattern of the array were made in reflection with a 0.8 mm diameter steel sphere serving as the target. The sphere was attached to a thin wire mounted parallel to the array axis and was mechanically scanned through the focal plane. The received R.F. signal was full-wave rectified and time-averaged over two periods of the pulse.

To accurately model the beam pattern of the array, the product of the transfer functions of the transmitting and receiving elements was measured using the procedure described in Section 2. The measurement was made in reflection with the target on the axis of the array. The received signal was digitized and the spectrum obtained with a standard F.F.T. algorithm.

In the first example, the central element of the array is used as the transmitter and an annulus of radius 0.7 cm as the receiver. A signal corresponding to $v(0,\bar{t})$ in equation (15) was measured with the target on the axis and placed 10 cm from the array. The received signal and its spectrum are plotted in Figure 6. Using the product of the

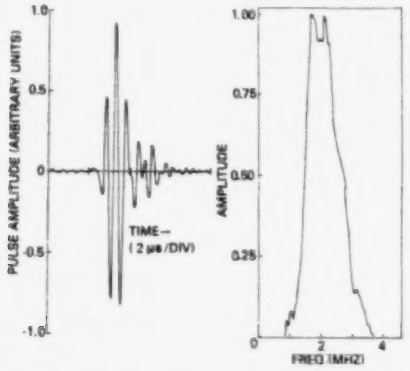


Fig. 6. Measured pulse shape and its spectrum.

transfer functions obtained in this measurement and the spatial factors for the piston and annulus, the off-axis response in the time domain, $v(\rho,\bar{t})$, can be calculated by taking the Fourier transform of equation (13). To model the measurement procedure, $v(\rho,\bar{t})$ is rectified and time-averaged over two periods of the pulse. The beam pattern calculated in this manner is shown with the solid curve in Figure 7. The dashed curve

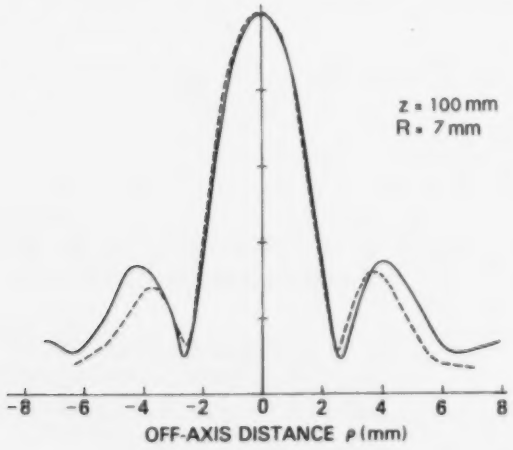


Fig. 7. Field pattern at 10 cm generated by a 0.4 cm diameter piston transmitter and a thin, 1.4diameter annulus, receiver. The solid line is the calculated response and the dashed line is the measured response.

corresponds to the measured beam pattern. The measurements are in close agreement considering that any non-uniformity in the transducer element will result in some deviation from the calculated result. (The model assumes an ideal annulus and piston.)

In the next example, we calculate the response for an annular array of 10 elements, with maximum radius of 1.6 cm, focused at 10 cm on both transmit and receive. To simplify the calculation, we assume that the product of the transfer functions for any two elements is the same. Thus, $F(\bar{\nu})$ and $G(\bar{\nu})$ can be factored out of the sums in equation (18). (This is a reasonable approximation for the array modeled here which has elements of similar size fabricated from a single plate.) The calculated response will then be the Fourier transform of:

$$V(\rho,\bar{\nu}) = F(\bar{\nu})G(\bar{\nu})\left(\sum_{i=1}^{n} H_{a_i}(\rho,\bar{\nu})\right)^2 , \qquad (24)$$

where the product $F(\bar{\nu})G(\bar{\nu})$ was determined in the first example. The calculated beam pattern for the focused array is plotted in Figures 8a and 8b on linear and logarithmic scales. The corresponding measured beam pattern is shown in Figure 9. The beam width and sidelobe levels of the calculated response are slightly smaller than the measured values. This would be expected assuming some deviations from the ideal response for the actual array elements. The overall agreement is good and the model accurately predicts the beam width and sidelobe levels.

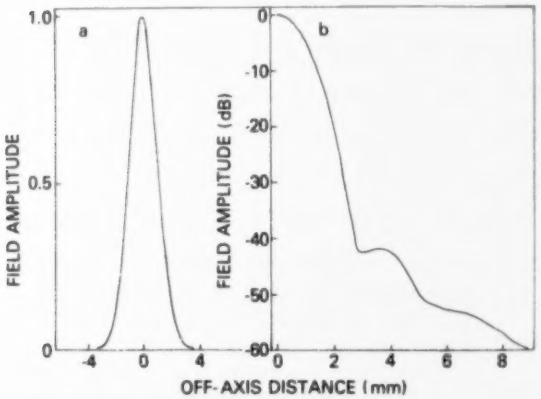


Fig. 8. Calculated response of the ten element, 3.2 cm o.d., annular array focused at 10 cm on transmit and receive.

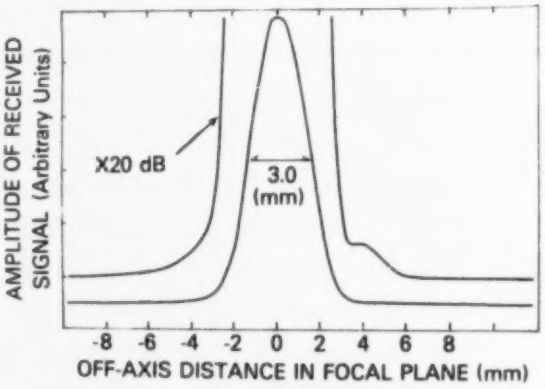


Fig. 9. Measured response of the ten element annular array focused at 10 cm on transmit and receive.

## 5. Conclusion

We have outlined an analytical model for calculating the response of a wideband annular array and have compared theoretical and measured results. The transfer functions of the transmitting and receiving transducers are incorporated into the description of the focal plane response. For the elements of an annular array, the required transfer function is determined by a single measurement with a reflector on the axis. The reflection measurement of the field pattern generated using a piston as the transmitter and an annulus as the receiver is in good agreement with the calculated field pattern. Likewise, the calculated response of the focused array compares well with the measured response. We have used the combined transmit-receive transfer function of one pair of elements to model the focused array. This appears to be a good approximation for an annular array with similarly sized elements. For more complex array geometries the transfer function of each element might have to be determined.

This model could serve as the basis for the synthesis of sparse arrays. Iterative techniques can be used to position array elements so as to minimize beam width and sidelobe level. The low sidelobes attained with the wideband array employed here would indicate that less dense array designs would have acceptable focal plane response. Some preliminary computer results support this conclusion.

## References


1. Dolph, C. L., "A Current Distribution for Broadside Arrays which Optimizes the Relationship Between Beam Width and Sidelobe Level," Proc. I.R.E. 34, 335-348 (1946).

2. Steinberg, B. D., Principles of Aperture and Array System Design, (John Wiley and Sons, New York, 1976).

3. Sherman, J. W., "Aperture-antenna Analysis" in Radar Handbook, M. Skolnik, ed., (McGraw Hill, New York, 1970).

4. Fung-I Tseng and D. K. Cheng, "Antenna Pattern Response to Arbitrary Time Signals," Can. J. Phys. 42, 1358-1368 (1964).

5. Miller, E. B., and F. L. Thurston, "Linear Ultrasonic Array Design for Echosonography," J. Acoust. Soc. Amer. 61, 1481-1491 (1977).

6. Stepanishen, P. R., "Wide Bandwidth Acoustic Near and Far Field Transients from Baffled Piston," in 1977 IEEE Ultrasonics Symposium Proceedings, (IEEE Cat. No. 77CH1264-1 SU), pp. 113-118.

7. Norton, S., and A. Macovski, "Broadband Focusing Through A Lens: A Linear Systems Approach," J. Acoust. Soc. Amer. (in press).

8. Goodman, J. W., Introduction to Fourier Optics, McGraw Hill, New York, 1969).

9. Dietz, D. R., S. Parks, and M. Linzer, "Expanding Aperture Annular Array," Ultrasonic Imaging, 1, 56-75 (1979).

## III. EXPANDING-APERTURE ANNULAR ARRAY

A dynamically-focused annular array system suitable for either contact or water-bath B-scanning has been developed. The design is based on a constant F-number approach, whereby, at short focal lengths, the aperture is increased in proportion to the focal length. This approach allows the use of larger area array elements, thus increasing the sensitivity of the system. Other major advantages include a substantial reduction in the time delays and refocusing rates required for the lens synthesis with a corresponding reduction in the electronic complexity of the system. The initial design employs an array operating at 2.25 MHz, with four annuli active at the near focal length of 1.5 cm. As the focal length increases, the array expands to a maximum of twelve rings, with 4.0 cm outer diameter, for focal lengths greater than 12 cm. A single, tapped delay line with 1 μs total duration provides the time delays for focusing on receive. A variable point or line focus is provided on transmit. Experimental measurements of the focusing properties of the system include beam profiles showing mainlobe width and sidelobe levels and B-scans of a standard test object.

### I. Introduction

In recent years, ultrasound pulse-echo imaging has become increasingly important in both nondestructive evaluation and medical diagnosis. Dynamic focusing techniques have improved the quality of imaging systems and the range of potential applications. Both one- and two-dimensional arrays are currently used in imaging systems. The one-dimensional array, or linear array, is the most convenient geometry for beam steering and focusing and has found its principal application in imaging rapidly-moving structures [1,2]. The linear array is capable of diffraction-limited resolution in the plane of the scan but provides poor resolution in the dimension perpendicular to that plane. Resolution in three dimensions requires the use of a two-dimensional aperture. Large aperture focused transducers have been shown to produce high quality images [3,4]. The simplest form of a two-

dimensional array is the annular array. An annular array, consisting of concentric annular rings, provides uniform azimuthal resolution about the axis of the array. When the array is dynamically focused on receive, the focus can be maintained over a large axial range. These arrays must be scanned mechanically in one dimension to produce a two-dimensional image, or B-scan. Motor-driven transducers or mirrors can be used to increase the frame rate to a value acceptable for real-time imaging [5].

Several designs for annular array focusing have been reported. The simplest form of an annular array is one consisting of an annulus, or axicon [6]. The field pattern of this single element is sharply peaked about the axis with a large depth of field but has relatively large side-lobes. It has been shown [6-8] that the field pattern of the annulus can be improved if it is segmented, with each segment appropriately weighted. The sensitivity of a focusing device of this design, however, is limited by the small area of the annulus. Superior performance, in terms of both sensitivity and focal plane response, can be achieved with multi-element annular arrays.

Previous designs of such systems have usually employed a fixed diameter array with the elements arranged in a Fresnel zone pattern [9,10]. The time delays required for wideband electronic focusing are generated either by lumped-constant delay lines, charge-coupled devices, or digital techniques. Implementation of the focusing electronics for such multi-element arrays is considerably more complicated than in the axicon case.

In this paper, we describe an expanding-aperture design approach whereby the diameter of the receiving array, at short focal lengths, is limited to that required to achieve the desired resolution. As the focal length increases during the A-scan, the aperture diameter increases, maintaining a constant F-number and hence a fixed beam width, until the full array is active. This design approach allows the use of large area array elements, thereby increasing the sensitivity of the imaging system. In addition, it results in a substantial reduction in the hardware required to focus the wideband array.

In the following section, we discuss the design considerations of an annular array including the factors that determine resolution and sensitivity. We then outline the constant F-number design approach and its effect upon such system parameters as element size and the time delays and refocusing

rates required for a dynamically-focused array. In Section III, we describe the imaging system built according to the constant F-number design approach. Measurements of the resolution of the imaging system, including beam profiles and B-scans of a standard test object, are presented in Section IV.

## 2. Annular Array Design Considerations

### A. Resolution

Before discussing the factors determining the resolution of an annular array, it is instructive to consider the focal plane response of a circular lens and a thin annulus. In the Fresnel approximation, the amplitude of the field in the focal plane of a circular lens is given by [11]

$$U_1(r) = \frac{2J_1(2\pi ar/\lambda z)}{(2\pi ar/\lambda z)} \qquad (1)$$

where $J_1$ is the first order Bessel function, $\lambda$ is the wavelength, a is the radius of the lens, z is the distance along the axis, and r is the off-axis

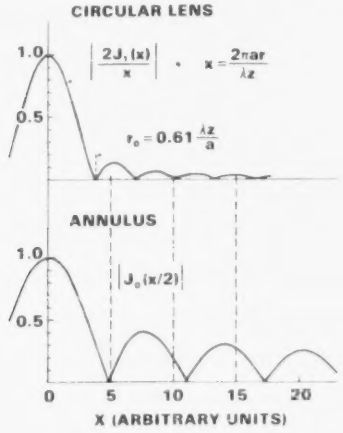


Fig. 1. Envelope of the focal plane response of a circular lens (top) and a thin annulus of one-half the lens diameter (bottom).

distance. The envelope of this pattern is plotted in Figure 1. The first zero of this field pattern occurs at an off-axis distance $r_o$, where

$$\begin{aligned} r_o &= 1.22\lambda(z/2a) \\ &= 1.22\lambda(\text{F-number}). \end{aligned} \qquad (2)$$

The F-number is defined as the ratio of the focal length to aperture diameter. The distance $r_o$ corresponds to the Rayleigh criterion for the minimum separation at which two point sources can be resolved. It is approximately equal to the width of the mainlobe at half-maximum amplitude and is proportional to the F-number of the lens. The first sidelobe of this circular lens pattern is 17 dB below the mainlobe and the amplitudes

of the higher order sidelobes decrease rapidly with off-axis distance. For comparison, we plot in Figure 1 the response, in the same plane, of a thin annulus with mean diameter equal to half the diameter of the lens. In this case, the amplitude of the response is proportional to the zeroth-order Bessel function, $J_o$. While the mainlobe is still relatively narrow, the sidelobes are much larger and decrease slowly with off-axis distance.

The field patterns shown in Figure 1 have been calculated for a single frequency model, and will be modified when wideband pulses, typical of those used in ultrasound imaging, are employed. In a pulse-echo imaging system, the resolution along the axis of the array (the range or longitudinal resolution) is determined by the pulse duration. The bandwidth of this pulse also affects the azimuthal field pattern (lateral resolution). The wideband focal plane response can be modeled by convolving the focal plane response of a lens, driven by an impulse, with the driving function [12]. The effect of the bandwidth on the focal plane response is readily seen in the example shown in Figure 2. Here, the measured beam patterns

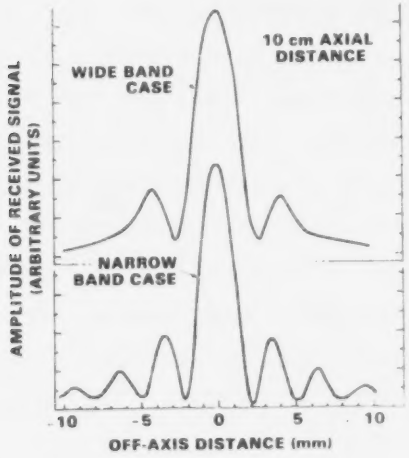


Fig. 2. Beam profiles for an annulus driven with a pulse of 40% bandwidth (top), and a single frequency waveform (bottom). The annulus has a radius of 11 mm and a width of 0.6 mm.

for an annulus from our array driven at a single frequency and in a pulsed mode with 40 percent bandwidth are compared. In the wideband case, the beam is somewhat broader and the sidelobes more widely spaced due to the lower frequency components present in the response of the pulsed transducer. The important difference between the two cases, however, is that in the wideband example, the sidelobes decrease rapidly with off-axis distance. At a point off-axis, energy arrives from various parts of the annulus at different times, thus spreading out the energy in the sidelobes in

the temporal dimension. Near the axis, the shape of the field pattern for the wideband case is similar to that in the single frequency example. Thus, we might expect that when signals from a large number of annuli are appropriately delayed and coherently summed, the focal plane response near the axis would approximate that of a circular lens at a single frequency. The Rayleigh criterion should thus provide an estimate of the diffraction-limited beam width. Further off axis, the lower sidelobes for the wideband annulus should result in lower sidelobes for the focused array than would be predicted by a single frequency model. The experimentally-measured beam patterns for our annular array, to be shown in Section IV, demonstrate this reduction in sidelobe level for the wideband case.

There are several factors which must be considered in selecting the F-number, and hence resolution, of a focused array. Equation (2) shows a linear relationship between the beam width in the focal plane and the array F-number. This linear relationship has been derived for the Fresnel region and is thus only valid for F-numbers on the order of 2 or more. For lower F-numbers, the resolution improves much more slowly with decreasing F-number. Usually, there are additional physical constraints on an imaging system which limit the useful aperture diameter, and hence the minimum F-number. These include the inhomogeneity of the medium under investigation, element directivity, and practical limits on the physical size of the aperture. Since the medium under examination is usually inhomogeneous, large effective path differences associated with a very low F-number array will result in phase errors and hence a deterioration in resolution. (The defocusing effects on an inhomogeneous medium on a lens system over a range of F-numbers has been described in a recent paper [13]). Elements fabricated from piezoelectric plates are not isotropic radiators, and their directivity becomes important at low F-numbers. In addition, the maximum aperture is often limited by the imaging environment. For example, in a contact scanner designed for materials inspection, the size of the transducer would be limited by the requirement that it make contact with the component. Thus, considering these limitations on the resolution attainable with an annular array for contact scanning, a minimum F-number of 2 is a practical design choice.

In a pulse echo imaging system, the same array is used to both illuminate the object and receive the reflected energy. For a narrow bandwidth imaging system, the response in any plane is simply the product of the transmit and receive field patterns. (While this is not strictly true for a wideband system, it provides a reasonable approximation for the response near the axis of an annular array system with a bandwidth on the order of 50 percent.) With a dynamically-focused receiver, a point focus can be achieved at all points along the array axis. On transmit, however, a single wavefront shape is produced for each pulse; but the transmitted energy can be concentrated along the axis, with a point or a weaker line focus, to further improve the focal plane response.

The field pattern of the wideband array can be further modified by apodizing the array as is done in narrow band antenna design [14]. Tapering the aperture function of a lens by decreasing the weighting near the edges results in a decrease in the widelobe level at the expense of widening the mainlobe. This aperture weighting can be accomplished by spacing or weighting the amplitude response of the individual array elements.

The field pattern of an annular array also depends upon the manner in which the outputs of the individual array elements are combined. The response for the circular lens shown in Figure 1 may be regarded as a model for a lineraly-processed dense array system in which the signals from the individual elements are coherently summed. The signals from the array elements may also be combined in a nonlinear fashion. For example, Welsby, *et al.*, [15], divided a linear array into two parts, processed each half in a linear fashion, and then multiplied the resulting signals. This multiplication of the diffraction patterns of the two segments resulted in a narrower mainlobe and lower sidelobes than for a linearly-processed array. Because a narrow bandwidth system was used, however, the presence of multiple targets or a target plus noise introduced artifacts resulting from cross-product terms. In a wideband imaging system, these cross-product terms may not be as serious a problem. Thurstone, *et al.*, [2], implemented nonlinear processing of a wideband array by logarithmically amplifying the signals from each array element prior to coherent summation. The logarithmic amplification served to compress the output dynamic range to a more acceptable value for visual

display. With this processing, they reported improved resolution and widelobe rejection without artifacts arising from multiple targets. In Section IV below, we will compare experimental results for linear processing with those obtained with a similar logarithmic processing technique.

B. Array Element Geometry

The sensitivity of an array is a function of the size of the individual array elements as well as the total active area of the array. Array elements with low width-to-thickness ratios will be less efficient in both transmit and receive due to coupling of the energy into unwanted modes of oscillation. Large elements should also be less susceptible to cross talk resulting from the mechanical contact between elements. In the receive mode, the equivalent source resistance of a piezoelectric plate is inversely proportional to its area, and thus the maximum attainable signal/noise ratio will be proportional to the square root of the element area. Therefore, within the constraints of the imaging system, element area should be maximized.

The geometry of the array element is determined by the focal range of interest. The maximum width of an annulus is calculated by requiring the phase shift across the element, with respect to any point

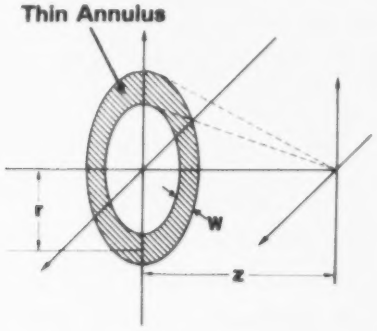


Fig. 3. Diagram of an annulus showing the path differences between the inner and outer edges with respect to a point on axis.

in the focal zone, not to exceed a certain maximum value. Referring to Figure 3, the phase shift, $\phi$, across an element of radius, r, and width, w, with respect to a source at a distance z along the axis is

$$\phi \approx \frac{2\pi}{\lambda} \frac{wr}{z(1+r^2/z^2)^{1/2}} \qquad (w<<zr)$$

$$\approx 2\pi wr/\lambda z. \qquad (r^2/z^2<<1) \qquad (3)$$

The maximum phase shift across the element occurs at the minimum focal distance. If we limit the maximum phase shift across an element to $\pi/2$, then eq. (3) can be written as

$$w \approx \lambda z_{min}/4r. \tag{4}$$

Thus, w is inversely proportional to r and, for $z_{min}$ a constant, all the array elements are of equal area. This geometry is known as a Fresnel zone plate and is commonly used for focusing at a single frequency. It is also the geometry that has been generally adopted [9,10] for wideband annular arrays, where $\lambda$ in eq. (4) refers to the center frequency of the pulse.

C. Dynamic Focusing

In a dynamically-focused annular array system, the returning echoes from each point along the axis are kept in focus by rapidly refocusing the array. To focus a wideband array, different time delays must be inserted in the signal paths of each array element prior to coherent summation.

There are several possible techniques for providing the delay and sum processing necessary for wideband, dynamically-focused imaging systems. These include lumped-constant delay lines, charged-coupled devices, serial analog memories, and digital techniques. Lumped-constant delay lines, interconnected by analog switches, provide accurate time delays and adequate bandwidths for systems operating in the 1-10 MHz frequency range. They are limited in dynamic range, however, by reflections from the taps and interconnections which are typically 30 to 35 dB below the signal level. Recent advances in charge-coupled devices and serial analog memory technologies have led to several other potential analog delay systems [16], but implementation of these devices is not trivial and the dynamic range available is comparable to or less than that of the lumped-constant delay lines in the frequency range of interest. Fully digital processing is becoming increasingly attractive as fast A/D converters become more readily available. The dynamic range and frequency of operation of the array system is then limited only by the resolution and speed of the A/D converter.

The time delay required to account for the path differences between the central element of a planar array and an annulus of radius r is

$$t = [(r^2 + z^2)^{1/2} - z]/c$$
$$= r^2/(2cz) \qquad (5)$$

where c is the velocity of sound in the medium. The largest time delay required is at the minimum focal length at which an element is active. Substituting z from eq. (4) into eq. (5), the maximum time delay can be written as a function of element radius and width, where $w_\lambda$ is the normalized width, $w/\lambda$, r has units of centimeters, and the velocity of sound used is that of water

$$t_{max} = (0.84\ r/w_\lambda)\ \mu s. \qquad (6)$$

When the array is dynamically focused on receive, these time delays must be readjusted during the A-scan. For a nominal signal frequency $f_o$, the difference in phase, $\theta$, between the wavefronts arriving at the center of the array and at an annulus of radius r is given by

$$\theta = \pi f_o r^2/cz \qquad (7)$$

The rate of change of $\theta$ is:

$$\left|\frac{d\theta}{dt}\right| = \pi f_o r^2/2z^2 \qquad (8)$$

If the array is refocused after each $\pi/2$ phase shift, the maximum refocusing rate, $f_s$, is given by:

$$f_s = f_o r^2/z^2. \qquad (9)$$

D. Constant F-number Design

In the constant F-number approach adopted here (Fig. 4), the active aperture diameter is varied during reception so as to maintain the

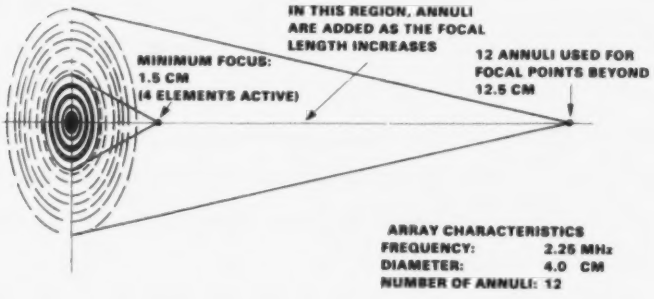
IN THIS REGION, ANNULI ARE ADDED AS THE FOCAL LENGTH INCREASES
MINIMUM FOCUS: 1.5 CM (4 ELEMENTS ACTIVE)
12 ANNULI USED FOR FOCAL POINTS BEYOND 12.5 CM
ARRAY CHARACTERISTICS
FREQUENCY: 2.25 MHz
DIAMETER: 4.0 CM
NUMBER OF ANNULI: 12

Fig. 4. Operation of the expanding-aperture array with dynamic focusing on receive.

desired F-number throughout the focal region. As the focal length increases, additional array elements are inserted in the focusing circuitry until the entire array is active. The major advantages of this approach are that it allows the use of larger area elements, thus increasing the sensitivity of the array, while substantially reducing the time delays and refocusing rates required for a dynamically-focused array.

The constant F-number design allows the use of elements of equal width rather than of equal area. Consider, for example, the outermost element of the array during a particular point in the receive cycle. Referring to eq. (4), we see that the width of the element is proportional to the ratio $(z_{min}/4r)$, where $z_{min}$ is the focal distance at which this element was activated. As the wavefront propagates further into the medium, the array is refocused and additional elements are activated such that $(z_{min}/2r)$ = F-number is maintained constant. Eq. (4) can then be expressed as

$$w_{max} = (\lambda/2)\text{F-number}. \qquad (10)$$

Thus, in a constant F-number design, the widths of all the elements added during the focusing operation are identical and are proportional to the F-number. For a Fresnel zone plate design, on the other hand, the widths of the elements are proportional to $1/r$. The active area of the expanding-aperture array then increases with the focal length as seems appropriate for measurements in an absorbing medium. For the same number of elements, this array will have a larger active area, and hence greater sensitivity for detecting distant targets.

As discussed above, an F-number of 2 appears to be a reasonable choice for an ultrasound scanner used for NDE of materials. For an F-2 system, we see from eq. (10) that the width of the annuli added to expand the aperture should be made equal to one wavelength. Assuming that the transducer is fabricated from a half-wave resonant piezoelectric plate and that the medium under investigation has a velocity comparable to that of water, then the width-to-thickness ratio of these elements would be approximately 0.6. While further reduction of the F-number may not significantly improve resolution, it will result in even lower width-to-thickness ratios, thereby decreasing the efficiencies of the elements.

The constant F-number approach also reduces the time delays and refocusing rates required for dynamic focusing. From eq. (6), the maximum time delay is seen to be proportional to the radius of an element

divided by its width. For a constant F-number array, the width is fixed and the maximum time delay is proportional to the array radius. For a design based upon a Fresnel zone plant, on the other hand, the width is inversely proportional to r and the time delay is proportional to the square of the array radius. For either design, the maximum refocusing rate [eqs. (8) and (9)] is inversely proportional to the square of the minimum F-number. Thus, limiting the F-number greatly reduces the rate at which the lens must be refocused and simplifies the implementation of dynamic focusing.

As an example, consider a conventional annular array system operating at 2.25 MHz with a fixed diameter of 4 cm and a minimum focus of 1.5 cm. Such an imaging system would require 6.7 μs of total time delay and a maximum refocusing rate greater than the signal frequency. A constant F-number system with an F-number of 2 would require 1.7 μs of delay and a maximum refocusing rate of 1/15th the signal frequency.

## III. System Design

A dynamically-focused annular array system has been constructed along the lines of the constant F-number approach described in the preceding section. The expanding-aperture array, shown schematically in Figure 4, was designed for use as either a contact or water-bath B-scanner. The array had a minimum F-number of 2 with dynamic focusing over a range of 1.5 to over 30 cm. An F-number of 2 could not be maintained over the entire region of interest because of practical limits on the aperture diameter. (The maximum diameter of the array was chosen to be 4 cm.) An F-number of 2 could then only be maintained for focal lengths up to 8 cm. To further reduce the hardware complexity of this prototype, the maximum time delay was limited to 1 μs, compared to a time delay of 1.7 μs required for an F-2, 4 cm diameter array. This resulted in an increase of the array F-number from F-2 to F-3 over the focal range of 5 to 12 cm. For focal lengths greater than 12 cm, the active array diameter was fixed and the F-number increased in proportion to the focal length.

The annular array was fabricated by a commercial supplier [17] according to our specifications. It was made from a lead metaniobate plate with a fundamental resonance of 2.27 MHz and was back-loaded to produce a 40 percent bandwidth. The nominal wavelength in water was approximately 0.7 mm. The array has twelve elements with a maximum diameter of 4 cm. The central four elements of the array are always

active and therefore were designed as a Fresnel zone plate, with equal area. The outer 8 elements were designed for a constant F-2 array and had widths equal to one wavelength. For ease of fabrication, the minimum separation between elements was one wavelength. Isolation between adjacent elements, when driven at a single frequency, was greater than 45 dB.

The operation of the array during a single A-scan may be understood by referring to Figure 5. The difference in propagation time through water from the focal point to each element of the array, relative to the central element, is plotted as a function of focal length. On the vertical scale, the time delay is in increments of 100 ns corresponding to approximately a $\pi/2$ phase shift. At the beginning of the A-scan, the focal length is adjusted to its minimum value of 1.5 cm and only the inner four elements of the array are activated. During the A-scan, the focal length is increased and additional annuli are activated whenever their time delay, relative to the central element, becomes less than 1.0 μs. For focal lengths greater than 12 cm, the entire array of twelve elements is active.

The array was weighted to yield uniform response from all active points on the aperture. On transmit, a voltage impulse was used to excite each annulus, and the transmitted voltage was adjusted so that the amplitude at a point on the axis was proportional to the area of a given annulus. On receive, the gain of each amplifier was weighted so that the amplitude of the received signal from a point on the axis was proportional to the area of the annulus. This apodization yielded better resolution than a tapered amplitude distribution; although the sidelobe levels were somewhat

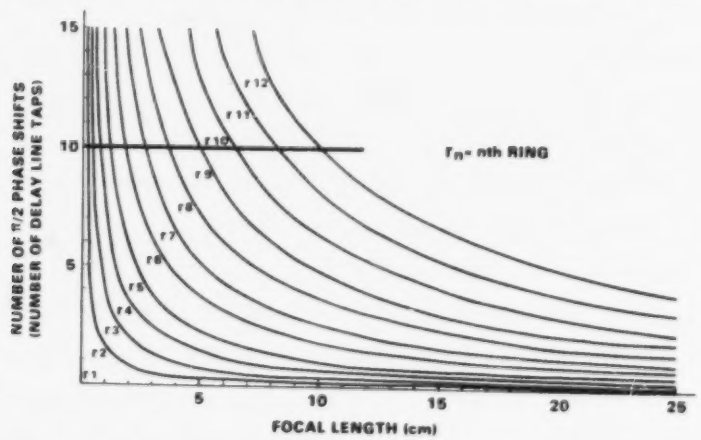


Fig. 5. Time delay relative to the central element required for each annulus as a function of focal length.

higher, they were considered acceptable for our application.

Figure 6 shows a block diagram of the delay line network used to provide the relative time delays required for dynamic focusing on receive. The output of each array element is amplified by either a linear or logarithmic amplifier and is multiplexed into the delay line. The output of the delay line is the coherent sum of the signals driving the individual taps. The delay line is of the lumped-constant type with a total delay of 1.0 μs, ten taps, and a bandwidth of 10 MHz.

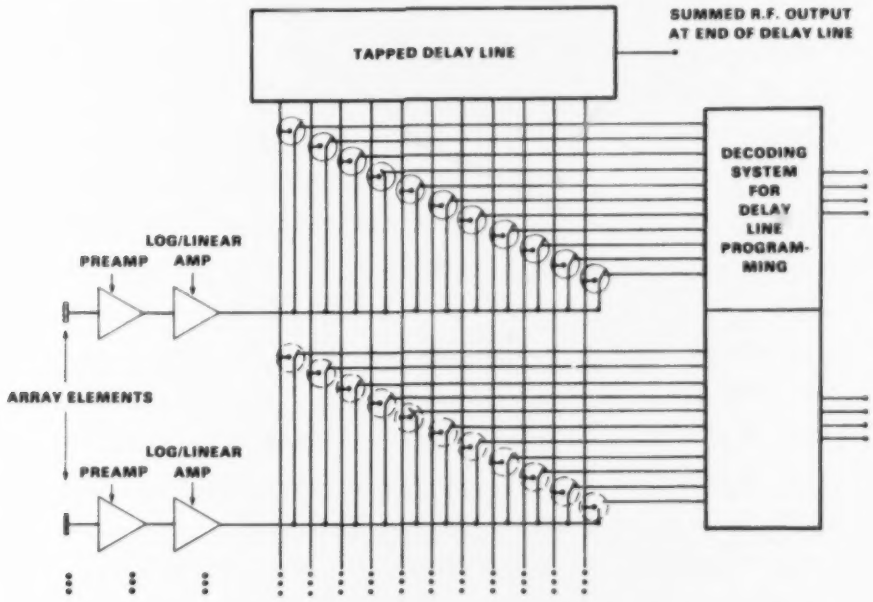


Fig. 6. Block diagram of the receiver amplifiers and analog multiplexer of the dynamically-focused array.

The circuit for multiplexing the R.F. signal from an array element into the delay line is shown in figure 7. Each array element drives a cascode amplifier with ten output stages. The bases of transistors $S_1 \ldots S_n$ are connected to the output of a decoder which activates one of the ten output stages. Thus, only one common base stage is turned on at a time, and a single transistor serves as the analog switch. Each tap is connected to the corresponding twelve outputs of the cascode amplifiers (points $A_i$) via a single cascode transistor. This transistor reduces spurious reflections in the delay line by minimizing capacitive and resistive loading at the taps.

During dynamic focusing, adjacent stages are switched with one transistor turned on as the other is turned off. Switching is accomplished with a time constant of approximately 1 μs to minimize switching transients.

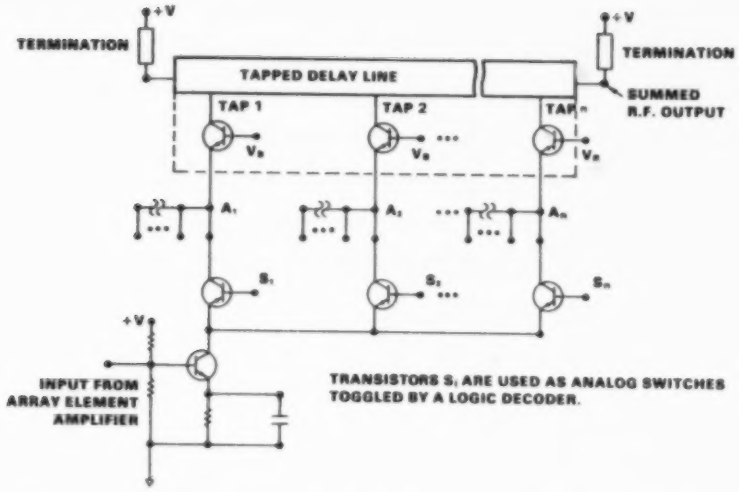


Fig. 7. Schematic diagram of the cascode amplifier-multiplexer circuit. Transistors Si are used as analog switches toggled by the logic decoder.

The switching sequence that drives the decoders is stored in a read-only memory that is clocked with a period of approximately 3 μs. The output dynamic range of the analog delay system, when all twelve rings are activated, is greater than 40 dB.

Figure 8 shows a block diagram of the circuit for generating the focal zone on transmit. A comparator is used to trigger the high voltage pulser of each array element. The $i^{th}$ tap on the resistor chain provides one voltage input of the $i^{th}$ comparator, while the other terminal of each comparator is driven by a voltage ramp. The relative firing time

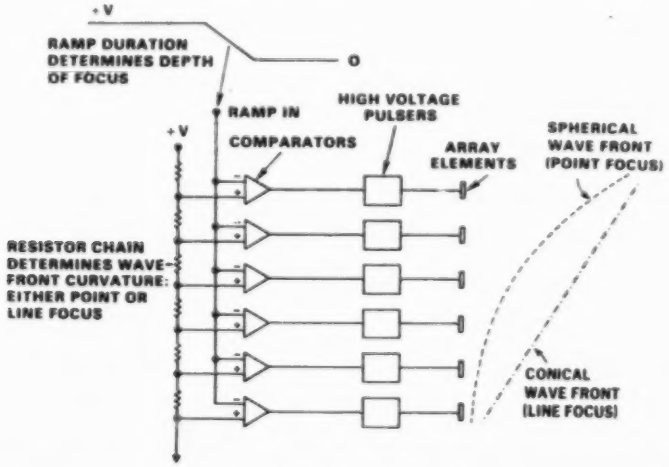


Fig. 8. Schematic diagram of the circuit used to generate a variable focus on transmit.

of the comparators determines the wavefront shape which is coded in the resistor chain. Resistor values are calculated so that the voltage difference between taps i and j is proportional to the difference between the firing times of the corresponding array elements. This time difference will be proportional to the difference in the square of the radii for a point focus, or to the difference in the radii for a line (axicon) focus [18]. Thus, for a point focus, the time difference between the firing of elements i and j is given by

$$t_i - t_j = \frac{V_i - V_j}{K} = \frac{r_i^2 - r_j^2}{2zc} , \qquad (11)$$

where $K = \frac{dV}{dt}$ is the ramp rate. Thus, when $(V_i - V_j)$ is proportional $(r_i^2 - r_j^2)$, the ramp rate, K, is proportional to the focal length, z.

## IV. Resolution Measurements

### A. Beam Profiles

Beam profiles for the annular array were measured in reflection in a water medium. A 0.8 mm diameter steel sphere served as a point reflector. The sphere was attached to a thin wire mounted parallel to the array axis and was mechanically scanned through the focal plane by means of a two-axis stepper-motor-controlled translator. The reflected R.F. signal was full-wave rectified and the video amplitude was measured with a sample-and-hold circuit using a 300 ns averaging window. This sampling circuit was triggered so that the window was centered on the received pulse when the target was positioned at the focus of the array. Beam widths and sidelobe levels were found to vary by only a few percent for averaging windows between 250 and 750 ns.

Beam profiles, measured at different focal distances, for the array focused to the same point on both transmit and receive are shown in Figures 9 and 10. The amplitude of the video signal is plotted as a function of the off-axis distance within the focal plane. For the 3 cm focal length, only the innermost six annuli (with aperture diameter of 1.7 cm) were active, while at the 15 cm focus all twelve annuli were in operation. The sidelobe levels throughout the 3 to 15 cm focal region were at least 30 dB below the mainlobe amplitude. Sidelobe levels in the 1.5 to 3 cm focal region were found to be at least 20 dB below the mainlobe level.

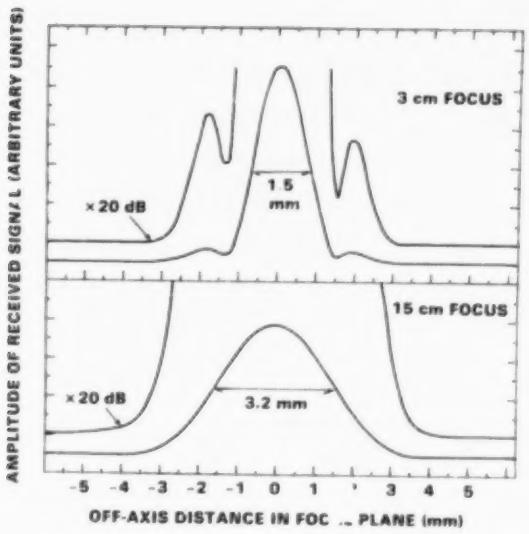
AMPLITUDE OF RECEIVED SIGNAL (ARBITRARY UNITS)
3 cm FOCUS
×20 dB
1.5 mm
15 cm FOCUS
×20 dB
3.2 mm
-5 -4 -3 -2 -1 0 1 3 4 5
OFF-AXIS DISTANCE IN FOC .. PLANE (mm)

Fig. 9. Beam profiles for the annular array focused on both transmit and receive at 3 and 15 cm.

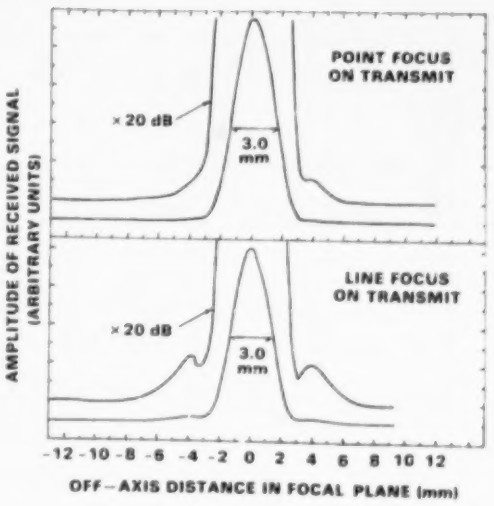
AMPLITUDE OF RECEIVED SIGNAL (ARBITRARY UNITS)
POINT FOCUS ON TRANSMIT
×20 dB
3.0 mm
LINE FOCUS ON TRANSMIT
×20 dB
3.0 mm
-12 -10 -8 -6 -4 -2 0 2 4 6 8 10 12
OFF-AXIS DISTANCE IN FOCAL PLANE (mm)

Fig. 10. Beam profiles for the annular array, focused on receive, comparing the use of a point or line focus on transmit.

In Figure 10, the beam profile for the array focused to a point on both transmit and receive is compared to that obtained with a line (axicon) focus on transmit and a point focus on receive. With the line focus, only a slight increase in beam width and sidelobe level is observed. However, outside the focal plane of the point focus on transmit, the sidelobe levels of the line focus are generally lower than those for the point focus. The combined transmit-receive response, over a larger focal region, is improved with the line focus on transmit.

The beam profiles shown in Figures 9 and 10 were obtained by linear processing of the outputs of the array elements. As discussed in Section II, the outputs can also be logarithmically compressed prior to coherent summation. The response of the imaging system, focused at 10 cm, with logarithmic processing prior to summation, is shown by the solid curve in Figure 11. If similar logarithmic compression is performed on the signal after coherent summation, the resulting beam profile is that of the dashed line in the figure. The logarithmic processing prior to coherent summation results in a narrower beam width and lower sidelobes than when logarithmic compression follows coherent summation. Some preliminary experiments were performed with two targets, separated by 2 mm in either the azimuthal direction or axial direction. No artifacts

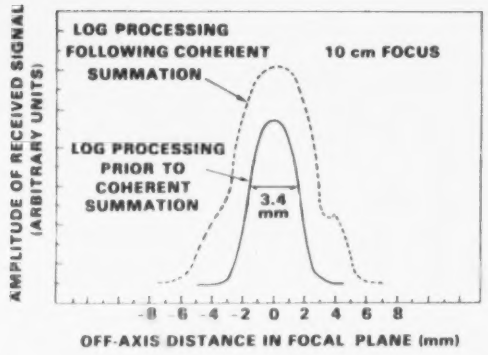


Fig. 11. Beam profiles for the annular array comparing the results of log processing before and after coherent summation. A point focus was generated on transmit.

were observed which could be attributed to this nonlinear processing. For more widely-spaced scatterers, interference effects due to nonlinear processing would not be expected given the short pulses employed and the rapid decrease in sidelobe level with off-axis distance.

In Section III, we described a technique for producing a variable point or line focus on transmit. This can be used as the basis for a minimal configuration electronic-focusing system consisting of the full array focused on transmit and a single annulus employed as the receiver. The focal plane response of such a system, at 10 cm, is shown in Figure 12. This focal plane response is acceptable for many imaging applications and can be further improved by apodizing the array on transmit.

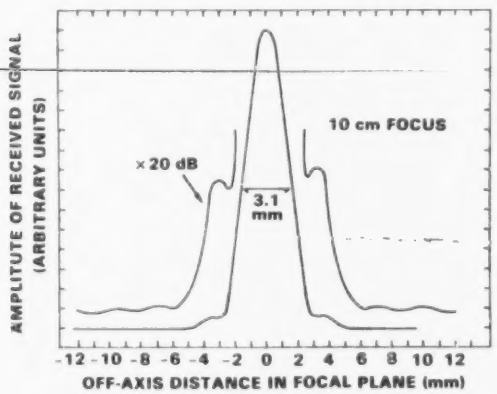
10 cm FOCUS
×20 dB
3.1
mm
AMPLITUTE OF RECEIVED SIGNAL
(ARBITRARY UNITS)
-12 -10 -8 -6 -4 -2 0 2 4 6 8 10 12
OFF-AXIS DISTANCE IN FOCAL PLANE (mm)

Fig. 12. Beam profiles for the array focused to a point on transmit with a 2.2 diameter annulus used as the receiver.

The advantage of dynamic focusing is that nearly diffraction-limited resolution can be maintained over a large axial range. In Figure 13, the solid line is the theoretical diffraction-limited beam width for a 4 cm diameter aperture, operating at 2.25 MHz and focused on both transmit and receive. (If a plane wave is transmitted and the array is focused on receive only, the beam width is increased by approximately a factor of $\sqrt{2}$.) A fixed-focus lens, however, can achieve diffraction-

limited resolution only over a small depth of field. We have modeled a fixed-focus lens by statically focusing the array, at a distance of 12 cm, on both transmit and receive. The dashed curve in Figure 13 represents the measured beam width for this case. While approximately diffraction-limited resolution is achieved at the focus, the useful depth of field is relatively small.

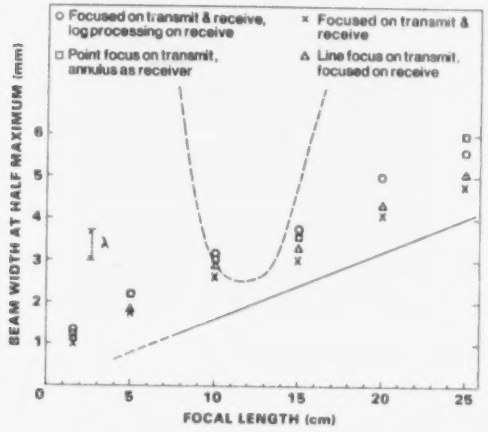


Fig. 13. Summary of resolution measurements with the focused annular array.

The data points plotted in Figure 13 represent the beam widths at half-maximum, obtained with the dynamically-focused array, for the several modes of operation previously described. The first set of data points is the measured beam width for the array focused at the same point on both transmit and receive. For an F-2 expanding-aperture array with a 4 cm maximum diameter, the beam width should be constant over the focal range of 1.5 to 8 cm. The second set of data points is the measured beam width when a line focus is produced on transmit. Only a slight increase in beam width is seen in comparison to that for a point focus on transmit. The third set of data points represents the beam width for the nonlinear processing mode. While the beam width is larger than in the case of linear processing, it is narrower than that obtained if similar logarithmic compression is employed following coherent summation. The fourth set of data points corresponds to the measured beam width for the minimal configuration system, employing the full array on transmit and a single annulus as receiver. For the data shown here, the receiving annulus had a diameter of 2 cm.

B. B-Scans of Standard Test Object

The expanding-aperture annular array system has been interfaced to a commercially-available B-scanner. This was accomplished by substi-

tuting the annular array for the single fixed-focus transducer in the scanner arm. The output of the array was fed into the A/D converter of the commercial unit. In Figure 14, compound scans of the AIUM test object

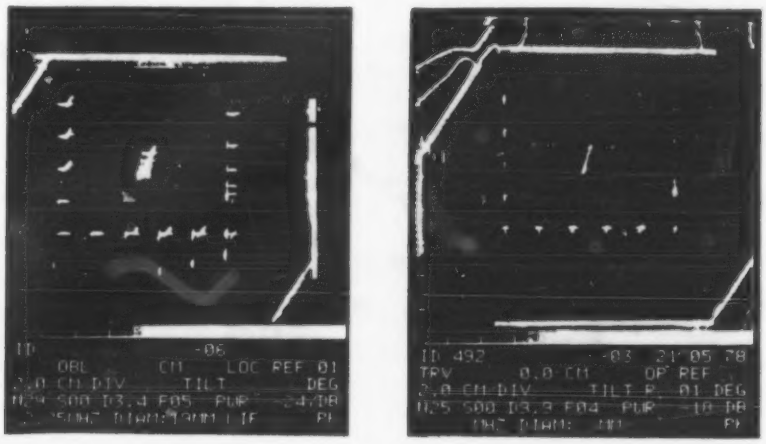

Fig. 14. B-scans of AIUM test object with a single, fixed-focus transducer (left) and with the dynamically-focused annular array (right).

[19] performed with the single, fixed-focus transducer and the dynamically-focused array are compared. The improved azimuthal resolution achieved with the array is clearly evident.

## V. Conclusions

The constant F-number annular array system described was shown to have several advantages over conventional designs [9,10]. Within the constraints of the resolution that is required, the area of the array elements is maximized while the signal processing to achieve this resolution is minimized.

Although not implemented in this work, this approach makes possible additional improvements that would result in increased array sensitivity. Lead metaniobate was chosen as the piezoelectric material for our array due to its low Q and low longitudinal-to-transverse coupling constants, two factors which affect the cross talk between elements. Because of the wide spacing and the large area of the elements in a constant F-number design, cross talk is reduced and more efficient ceramic transducers, such as PZT 5A, might also be used effectively. Further increases in transducer efficiency may be achieved by the use of multiple matching layers [20,21]. Matching layers serve to couple the transducer more efficiently to the medium and to increase its bandwidth. The design of

the matching layers, however, is based upon a thin plate model and is strictly valid only for large width-to-thickness ratios. The large area elements associated with a constant F-number design would allow more effective transducer matching. Further developments along the lines of more efficient array design might also include the use of a fixed lens [22] or spherical surface [23] in conjunction with the expanding-aperture array. This would allow the use of even larger array elements and a further reduction in signal processing.

The expanding-aperture array was shown to have excellent focal plane response. The narrow beam widths and low sidelobe levels result from the radiation patterns of the relatively large, widely spaced array elements and the wideband character of the pulse employed. Our results indicate that, with linear processing and some apodization, sidelobe levels 40 dB below the mainlobe can be obtained. The use of nonlinear processing also appears to have some advantages in decreasing the beam width when dynamic range compression is required.

Appendix - Supplementary Circuit Documentation

Figure 15 shows one of the twelve impulse generators used in the transmit circuit. A chain of fast SCR's discharge a capacitor, producing a pulse with a rise time on the order of 100 ns.

The preamplifier is shown in Figure 16. Its input is guarded from the high voltage pulser by the diode protection circuit. The first stage is a low noise FET followed by an r.f. amplifier with AGC capabilities. The gain of this amplifier is approximately 50 dB. The linear/logarithmic amplifier is shown in Figure 17. The input stage has a gain of 30 dB. The logarithmic section has an output dynamic range of approximately 18 dB. Switching between the linear and logarithmic sections is done by means of PIN diodes.

Figure 18 is a diagram of the digital control circuit for driving the decoders. For each array element there is a 4-bit memory, data latch, and decoder to select the appropriate tap of the delay line. The memory addresses are wired in parallel and driven by an address counter. The focusing sequence is calculated and stored in the memory. For this prototype, a CMOS random access memory with a battery backup was used so as to be easily reprogrammed. The output of the 2-phase clock updates all the data latches every 3 μs to refocus the array.

Figure 19 is a schematic diagram of the address counter. The 7437 line drivers control the address lines of all twelve memories. The decoder and switch drivers are shown in Figure 20. Only 300 mv voltage swing is required to toggle the transistor switches, $S_i$, in Figure 7.

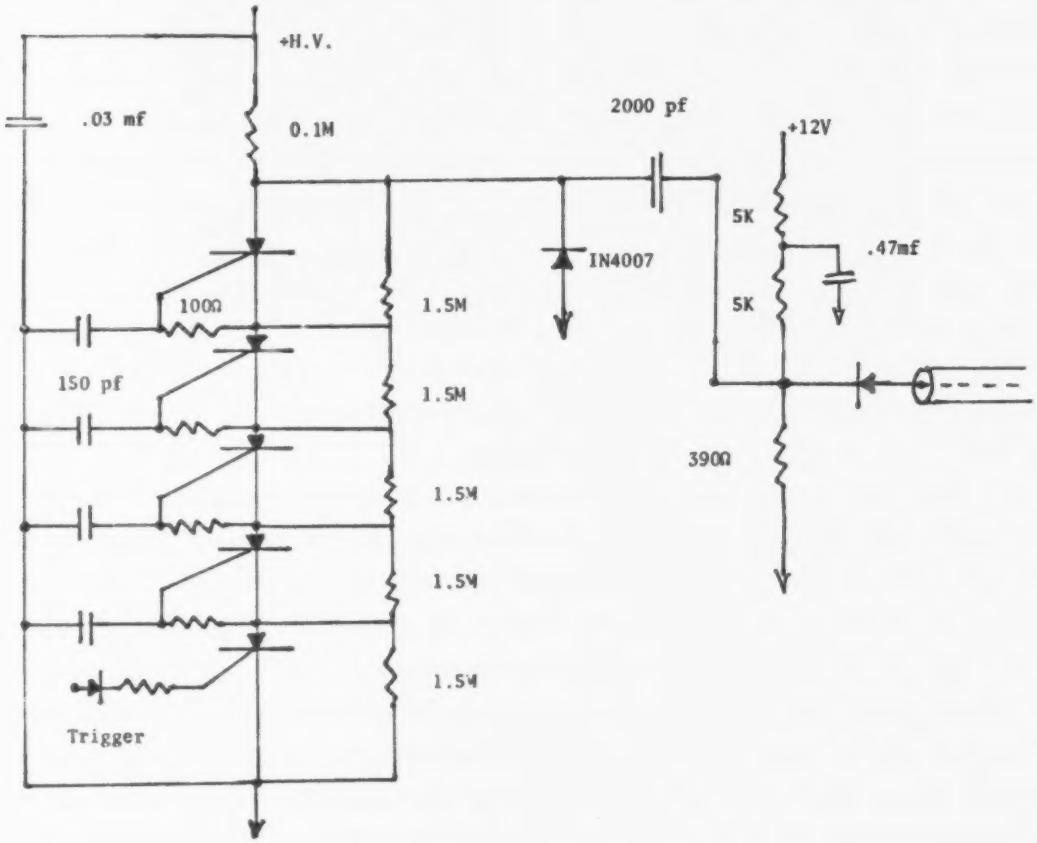


Fig. 15. High voltage pulser.

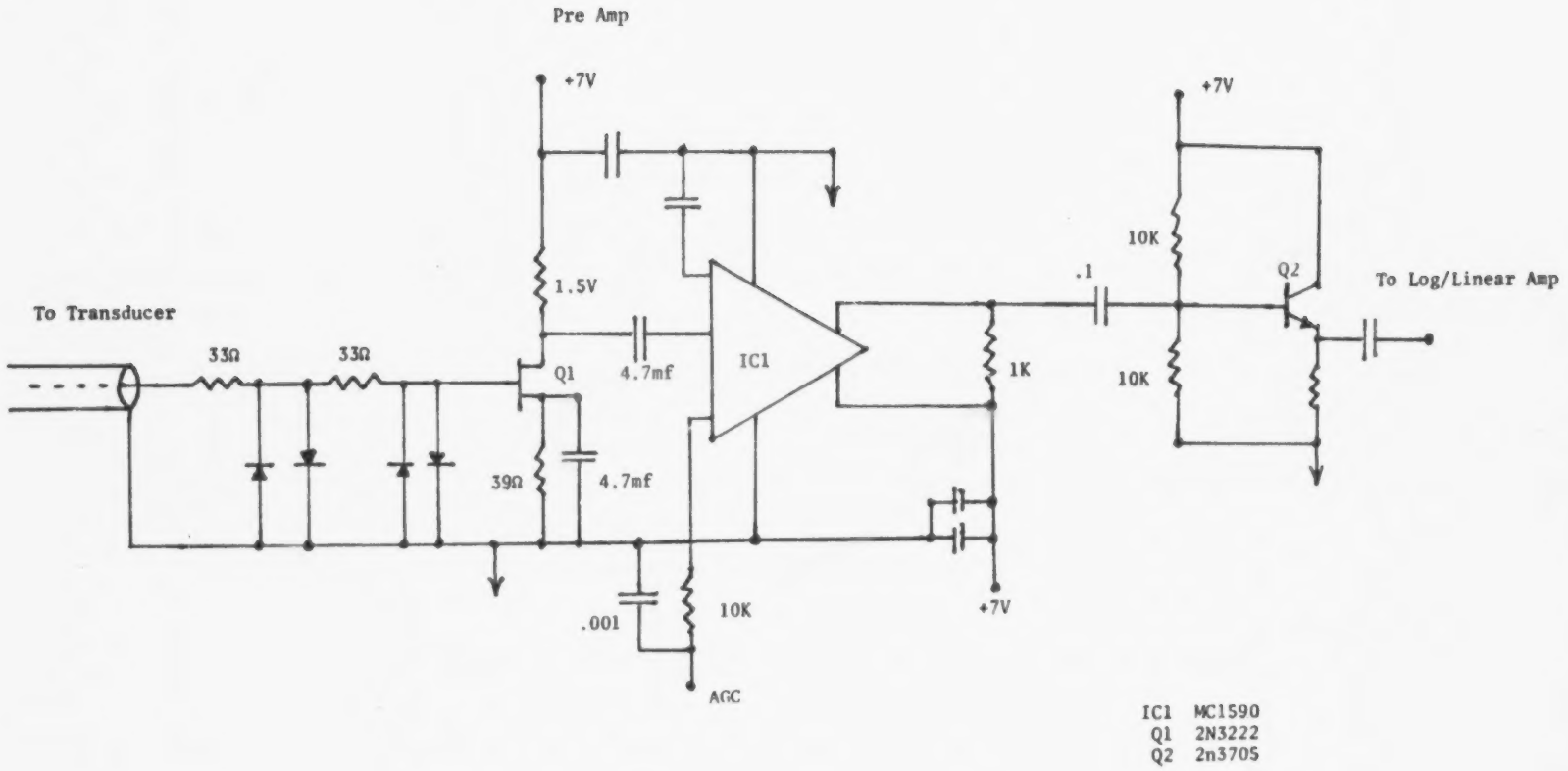


Fig. 16. Preamplifier.

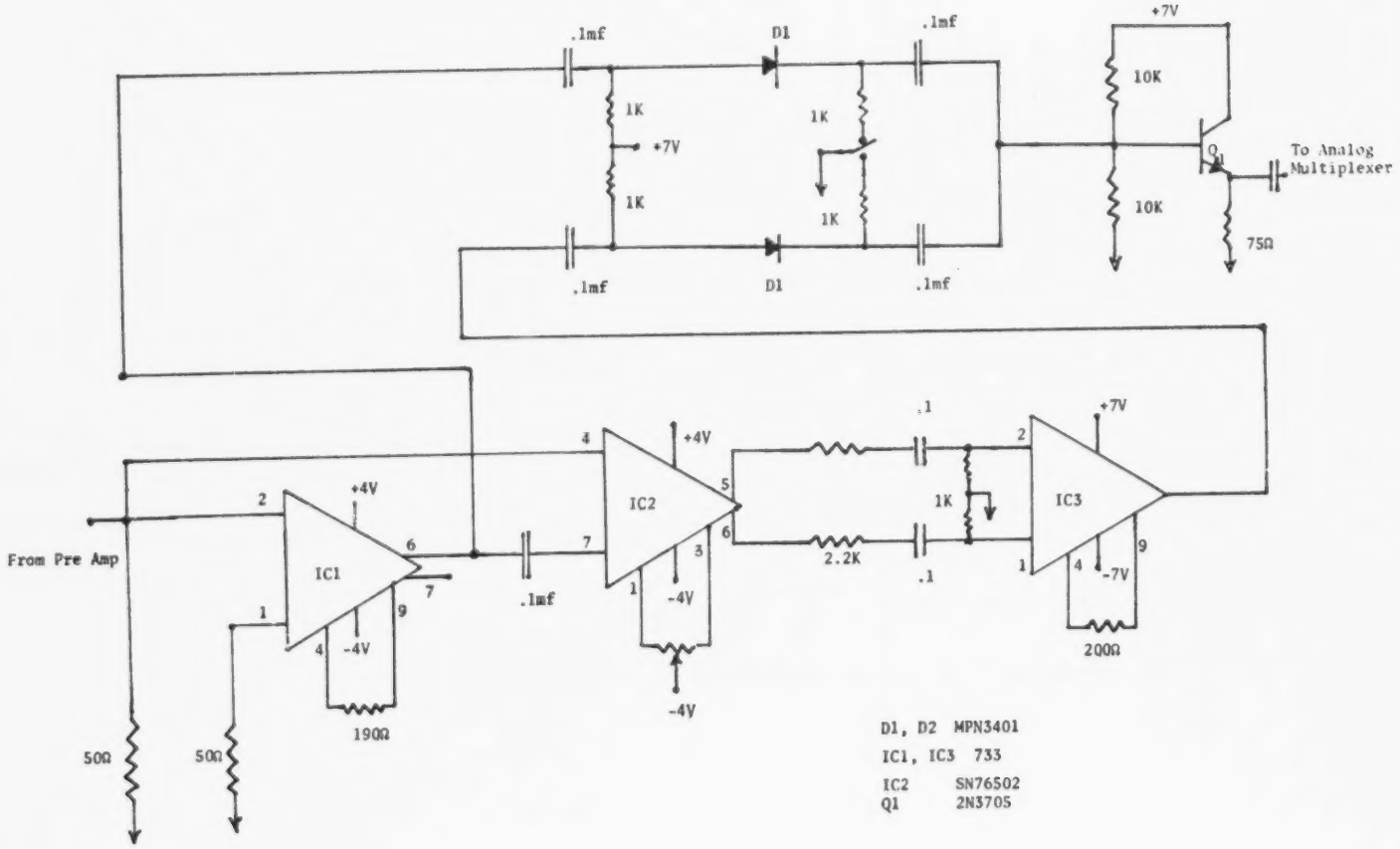


Fig. 17. Log/linear amplifier.

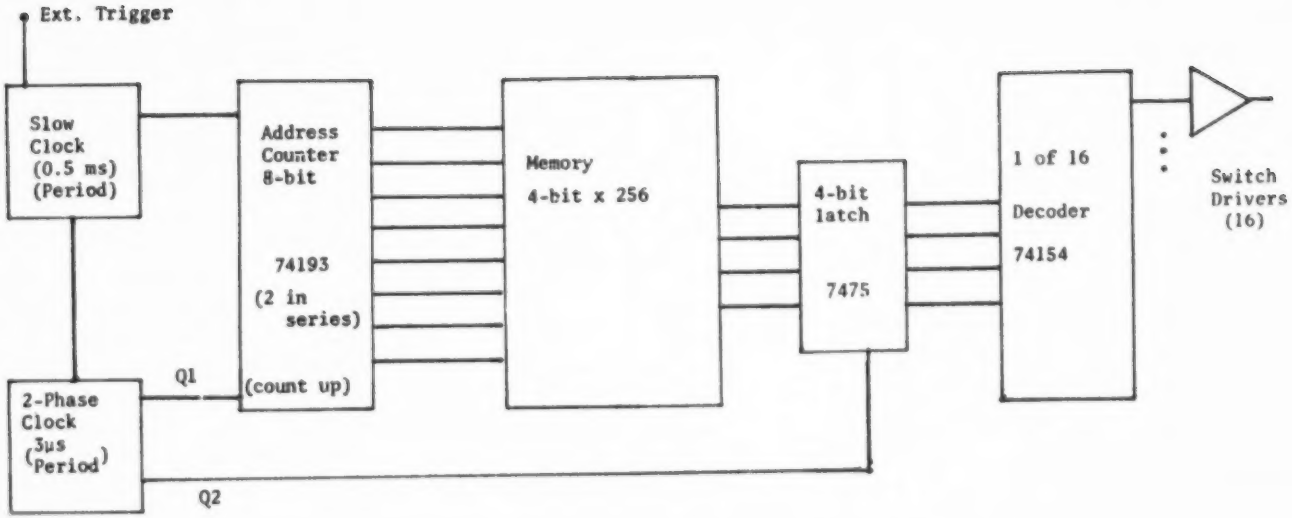


Fig. 18. Block diagram of digital control for the fast analog multiplexer.

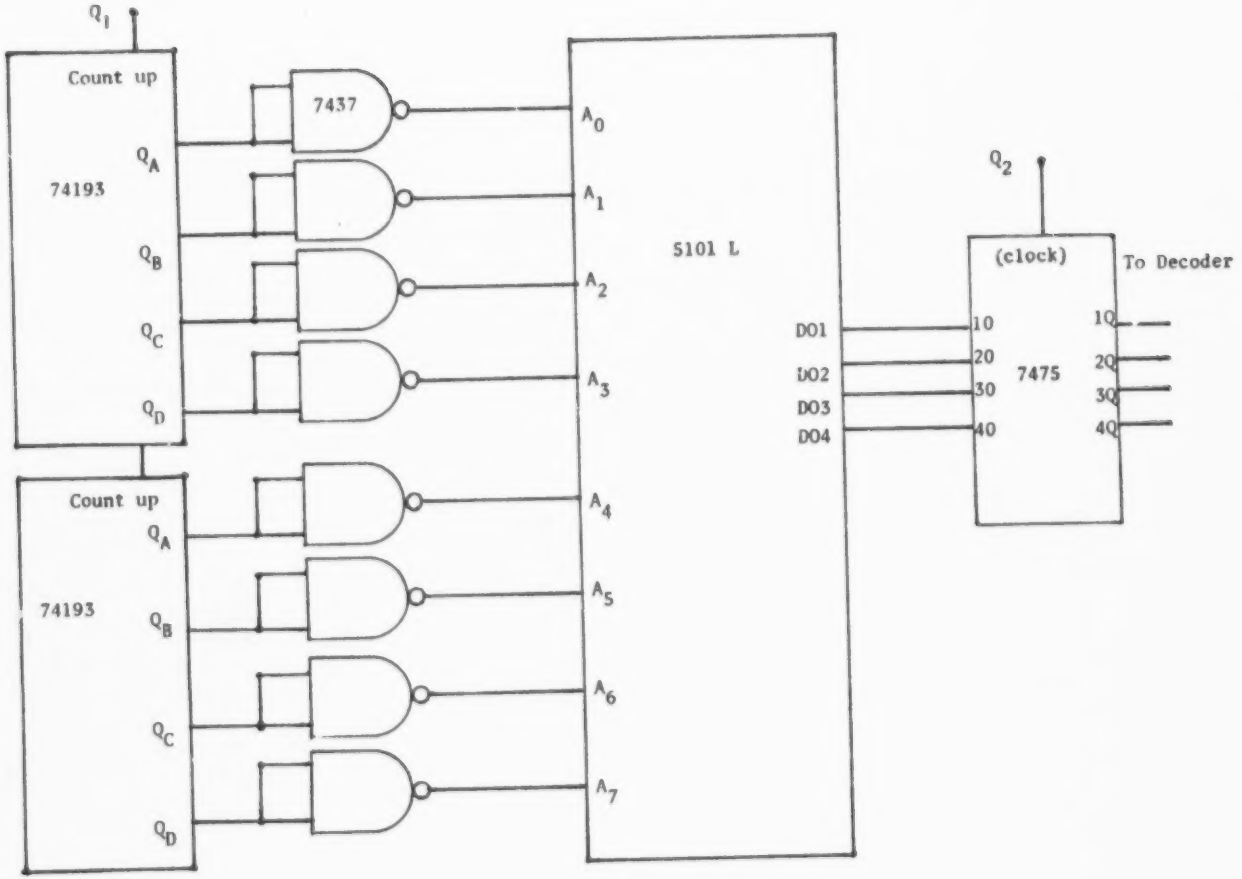


Fig. 19. Address counter and memory.

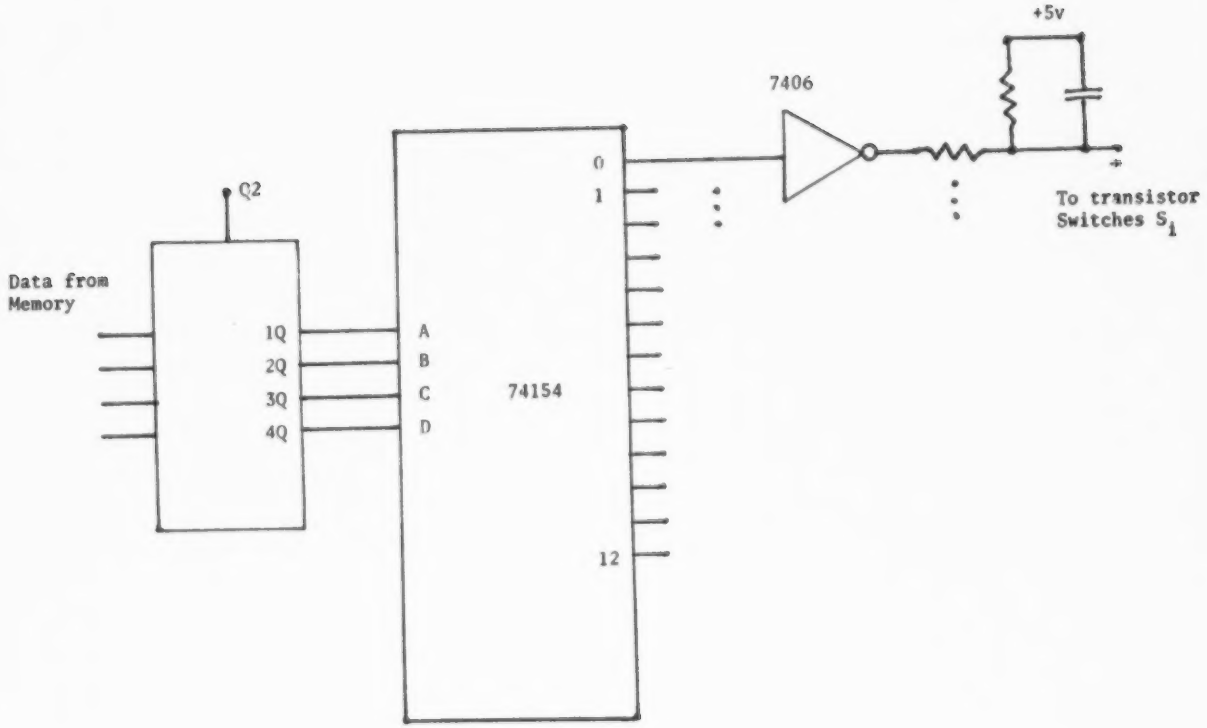


Fig. 20. Decoder and switch-driver circuit.

References


1. von Ramm, O. T., and Thurstone, F. L., Cardiovascular Diagnosis with Real Time Ultrasound Imaging, in Acoustical Holography, Vol. 6, Newell Booth, ed., pp. 91-102 (Plenum Press, New York, 1975).

2. Thurstone, F. L., and von Ramm, O. T., New Ultrasound Imaging Technique Employing Two-dimensional Electronic Beam Steering, in Acoustical Holography, Vol. 5, Philip Green, ed., pp. 249-259 (Plenum Press, New York, 1974).

3. Kossoff, G., Carpenter, D. A., Radovanovich, G., Robinson, D. E., and Garrett, W. J., Octoson: A New Rapid Multitransducer General Purpose Water-coupling Echoscope, in Ultrasonics in Medicine, E. Kazer, M. de Vlieger, H. R. Muller, and V. R. McCready, eds., pp. 90-102 (American Elsevier, New York, 1975).

4. Garrett, W. J. Kossoff, G., and Fisher, C., Ultrasonic Diagnosis of Congenital Abnormalities in the Fetal Chest and Abdomen, in Ultrasonics in Medicine, E. Kazner, M. de Vlieger, H. R. Muller, and V. R. McCready, eds., pp. 311-315 (American Elsevier, New York, 1975).

5. This approach has been taken in several commercial units.

6. Vilkomerson, D., Acoustic Imaging with Thin Annular Apertures, in Acoustical Holography, Vol. 5, Philip Green, ed., pp. 283-316 (Plenum Press, New York, 1974).

7. Burckhardt, C. B., Grandchamp, P.-A., and Hoffman, H., Focusing ultrasound over a large depth with an annular array transducer--an alternative method, IEEE Trans. Sonics and Ultrasonics, SU-22, 11-15 (1975).

8. Macovski, A., and Norton, S. J., High Resolution B-Scan Systems Using a Circular Array, in Acoustical Holography, Vol. 6, Newell Booth, ed., pp. 121-143 (Plenum Press, New York, 1975).

9. Melton, H. E., and Thurstone, F. L., Annular array design and logarithmic processing for ultrasonic imaging, Ultrasound Med. Biol., 4, 1-12 (1979); Melton, H., Electronic Focal Scanning for Improved Resolution in Ultrasound Imaging, Ph.D. Thesis, Duke University, 1972 (University Microfilms Cat. No. 72-23, 243).

10. Bernardi, R. B., Peluso, P. J., O'Connell, R. J., Kellog, S., and Shih, C., A Dynamically Focused Annular Array, 1976 IEEE Ultrasonics Symposium Proceedings, pp. 157-159 (IEEE Cat. No. 76 CH1120-5SU).

11. Goodman, J. W., Introduction to Fourier Optics, (McGraw Hill, New York, 1968).

12. Norton, S. J., Theory of Acoustic Imaging, Ph.D. Thesis, Stanford University, 1976.

13. Foster, F. S., and Hunt, J. W., The Focusing of Ultrasound Beams Through Human Tissue, in Acoustical Holography, Vol. 8 (Plenum Press, New York) (in press).

14. Steinberg, B. D., Principles of Aperture and Array System Design (John Wiley and Sons, New York, 1976).

15. Welsby, V. G., Multiplicative receiving array--the angular resolution of targets in a sonar system with electronic scanning, J. Brit. I.R.E., 22, 5-12 (1961).

16. Walker, J. T., and Meindl, J. D., A Digitally Controlled C.C.D. Dynamically Focused Phase Array, 1975 IEEE Ultrasonics Symposium Proceedings, pp. 80-83 (IEEE Cat. No. 75 CHO 994-4SU).

17. Dapco Industries, Inc., Georgetown, CT, 06829. (Certain commercial equipment, instruments, or materials are identified in this paper in order to adequately specify the experimental procedure. In no case does such identification imply recommendation or endorsement by the National Bureau of Standards, nor does it imply that the material or equipment identified is necessarily the best available for the purpose.)

18. Burckhardt, C. B., Hoffman, H., and Grandchamp, P.-A., Ultrasound axicon: A device for focusing over a large depth, J. Acoust. Soc. Amer., 54, 1628-1630 (1973).

19. Erickson, K. R., and Carson, P. L. (primary authors), The AIUM standard 100 mm test object and recommended procedures for its use, Reflections, 1, 74-91 (1975).

20. Auld, B. A., Drake, M. E., and Roberts, C. G., Monolithic acoustic imaging transducers with high spatial resolution, Appl. Phys. Letters, 25, 478-479 (1974).

21. DeSilets, C. S., Fraser, J. D., and Kino, G. S., The design of efficient broadband piezoelectric transducers, IEEE Trans. Sonics and Ultrasonics, SU-25, 115-125 (1978).

22. Green, P. S., Havilice, J. F., Holzemer, S. D., Ramsey, J. R., Taenzer, J. C., and Moessner, H. Z., Design and construction of a dynamically focused annular array, IEEE Trans. Sonics and Ultrasonics, SU-25, 259 (1978) (Abstract only).

23. Ueda, M., Sato, T., and Maeda, Y., Dynamic focusing ultrasonic transducer by using analog gate delay circuits, Bull. Tokyo Inst. Tech., 119, 55-63 (1973).

## IV. SPATIAL-TEMPORAL AVERAGING

In the previous fiscal year, the use of the NBS ultrafast signal averager to increase signal-to-random noise ratio in ultrasonic NDE was demonstrated. In the case of inspection of austenitic steel, a point was reached where the background or grain noise became dominant and further improvement in sensitivity could not be obtained by signal averaging. In this fiscal year, a series of experiments was undertaken to determine the

efficacy of spatial-temporal averaging in reducing the grain noise in austenitic steel components. In this approach, short-term averaging is employed as the transducer is moved over the structure of interest. Signals arising from grain scattering change rapidly with transducer position and tend to average out to either zero or to a constant d.c. level, depending on whether r.f. or detected signals are observed. A signal from an extended flaw, on the other hand, would be approximately constant over a limited range of transducer motion and thus would increase in amplitude over that from grain scattering.

Because of its unique high-speed capability, the NBS averager was investigated as a potential tool for practical implementation of spatial-temporal averaging in field applications. Using this device, an operator could move the transducer fairly rapidly over the surface of a component and still average sufficient signals to reduce grain noise.

To test the efficacy of spatial averaging, two different test configurations were studied. In one of these, a transducer was moved parallel to an extended flaw, thus providing optimum signal-to-noise enhancement. This situation could obtain in practice if a flaw were located and its orientation determined; spatial averaging could then be employed to determine its exact shape and size. The other test configuration corresponded to a worst case situation -- that of searching for a small flaw in the presence of grain noise.

The first series of experiments were carried out in collaboration with Dr. H. Wustenberg from BAM, Berlin, West Germany, and the second series with Dr. K. Goebells from the Institut für Zerstorungsfreie Prufverfahren, Saarbrucken, West Germany. Both the samples and transducers were provided by these laboratories; Drs. Wustenberg, Goebells, and Mohr (also from the Saarbrucken laboratory) participated in the experiments during visits to NBS.

A. Spatial-Temporal Averaging from Extended Flaws

The specimen (Fig. 1) was a block (50 x 70 x 120 mm) with six side-drilled holes of different depths and lengths. The diameters of all the holes were 3 mm. The transducers were especially developed, under license to BAM, for maximizing the flaw signal-to-grain noise ratio. They each consisted of transmitter-receiver probes designed for inclined longitudinal waves of 2 MHz frequency and 45° angle of incidence (Fig. 2). They

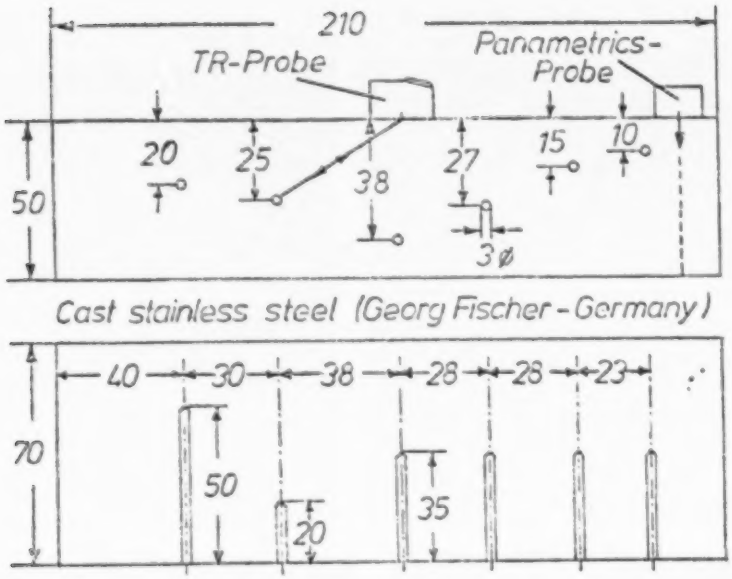


Fig. 1 Specimen configuration for spatial-temporal averaging of signals from extended flaws.

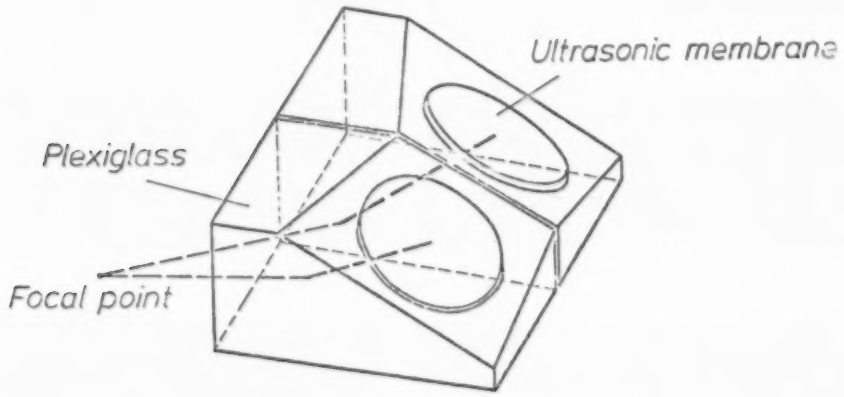


Fig. 2 Schematic diagram of transmitter-receiver probes.

were highly-damped (thus frequency averaging the grain signals) and were adopted for the different depths of the side-drilled holes by adjustment of the crossover points of the transmit and receive beams. The probes were manually moved parallel to the axis of the side-drilled holes using another steel block for guidance. This probe/specimen configuration provided optimum conditions for spatial-temporal averaging and could thus be used to set an upper limit on what could be achieved in practice.

A commercial device (Panametrics Model 5050PR [1]) was used as the transceiver. The received r.f. signal was fed into the NBS averager and 1024 averages were taken. This corresponded to 1 second of averaging at the maximum 1 KHz repetition rate of the Panametrics unit.

Figures 3-5 show a comparison of A-scans from unaveraged and averaged signals from the side-drilled holes at three different depths while Figure 6 shows the first and second backwall reflections using a commercial, 5 MHz center frequency, broadband probe. The results, summarized in Table 1, demonstrate that spatial-temporal averaging provides a maximum improvement of 4-5 dB.

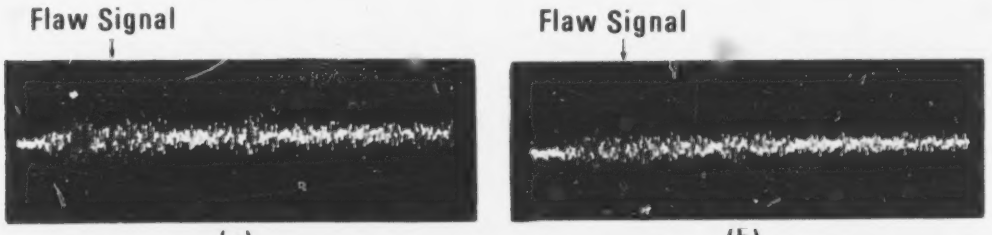


Fig. 3

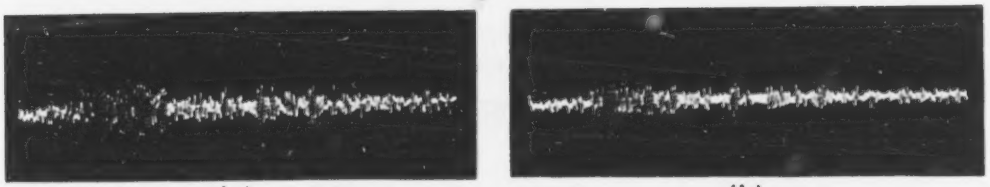


Fig. 4

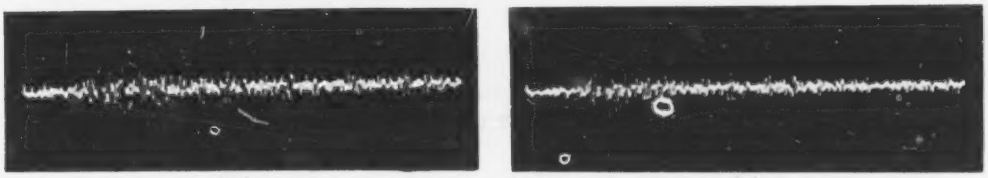


Fig. 5

Figs. 3-5 Single (a) and averaged (b) A-scan signals showing reflections from 3 mm diameter side-drilled holes at depths of 38 mm (Fig. 3), 27 mm (Fig. 4), and 25 mm (Fig. 5).

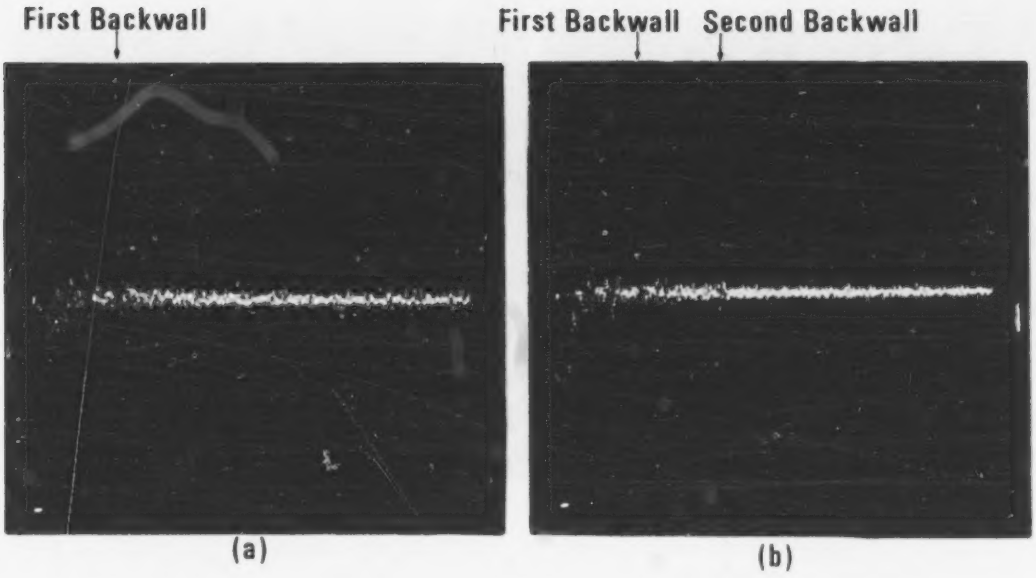


Fig. 6 Single (a) and averaged (b) A-scans showing reflections from backwall of austenitic steel block.

B. Spatial-Temporal Averaging from Small Flaws

The second series of experiments were performed on a 2.8 cm thick block of austenitic steel containing a 1 mm diameter flat-bottom hole. The hole was drilled from the backside of the specimen to a depth of 5 mm, so that there was no confusion between the flaw and backwall echoes. A 5 MHz longitudinal-wave unfocused transducer was used in conjunction with the Panametrics unit. A small circle was drawn on the upper surface of the specimen directly over the drilled hole and the transducer was moved manually over a random path within the circle. A total of 256 averages were taken. The undetected r.f. tended to average out to zero for both flaw and grain signals as the transducer was moved in the circle. All experiments thereafter employed detection prior to averaging.

A-scan signals from the flaw region were compared for a single scan and scans averaged without transducer motion. The pictures were nearly identical for the two cases.

A representative single A-scan and A-scan obtained after averaging, obtained in the flaw region, are shown in Figure 7. The flaw and interference signals in the averaged A-scan case are seen to be reduced by about

TABLE 1

| Figure | Probe | Reflector | Diameter (mm) | Depth (mm) | S/N(dB) |
|---|---|---|---|---|---|
| 3a | 45°, 2 MHz longitudinal-wave broadband, transmit/receive probes (see Fig.2) | side-drilled holes | 3 | 38 | 5.0 |
| 3b | | | | 38 | 7.0 |
| 4a | | | | 27 | 7.8 |
| 4b | | | | 27 | 12.0 |
| 5a | | | | 25 | 6.6 |
| 5b | | | | 25 | 9.0 |
| 6a | Panametrics, 5 MHz 0° longitudinal-wave broadband, 12.5 mm diameter | backwall | | 50 (1st reflection) | 1st - 16.0<br>2nd - 0 |
| 6b | | | | 100 (2nd reflection) | 1st - 19.6<br>2nd - 5.0 |

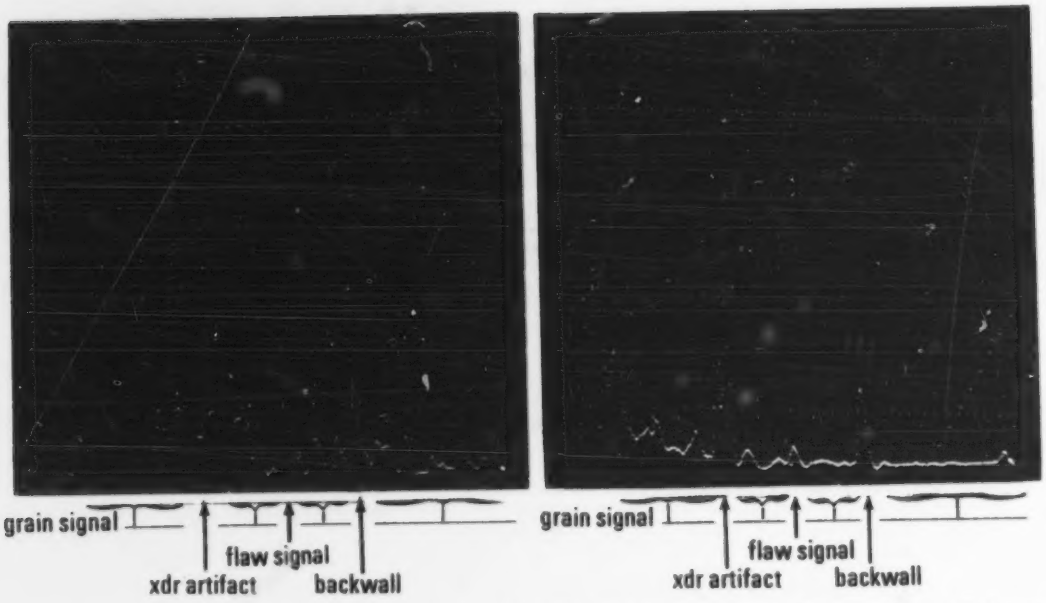


Fig. 7 Single (a) and averaged (b) A-scan signals in region of 1 mm flat bottom hole.

the same degree so the signal-to-background noise ratio was not affected by the averaging. Changing the pattern of transducer motion or increasing the number of averages did not change this picture substantially.

C. Summary

The results of our experiments show that spatial-temporal averaging would be effective in the case of large flaws whose orientation is approximately known. Even so, one cannot expect a signal-to-noise improvement beyond 4-5 dB. In the case of very small flaws, spatial-temporal averaging did not appear to improve the detection sensitivity.

---

(Certain commercial equipment, instruments, or materials are identified in this paper in order to adequately specify the experimental procedure. In no case does such identification imply recommendation or endorsement by the National Bureau of Standards, nor does it imply that the material or equipment identified is necessarily the best available for the purpose.)

NRC FORM 335 (7-77) U.S. NUCLEAR REGULATORY COMMISSION

**BIBLIOGRAPHIC DATA SHEET**

1. REPORT NUMBER (Assigned by DDC): NUREG/CR-1076

2. (Leave blank)

3. RECIPIENT'S ACCESSION NO.

4. TITLE AND SUBTITLE (Add Volume No., if appropriate)
Development of High-Sensitivity Ultrasonic Techniques for In-Service Inspection of Nuclear Reactors

5. DATE REPORT COMPLETED
MONTH: November YEAR: 1978

7. AUTHOR(S)
M. Linzer and others

DATE REPORT ISSUED
MONTH: November YEAR: 1979

9. PERFORMING ORGANIZATION NAME AND MAILING ADDRESS (Include Zip Code)
Center for Materials Science
National Measurement Laboratory
National Bureau of Standards
Washington, DC 20234

6. (Leave blank)

8. (Leave blank)

12. SPONSORING ORGANIZATION NAME AND MAILING ADDRESS (Include Zip Code)
Metallurgy & Materials Research Branch
Division of Reactor Safety Research
U.S.N.R.C.
Mail Stop 1130 SS
Washington, DC 20555

10. PROJECT/TASK/WORK UNIT NO.

11. CONTRACT NO.
AT(49-25)9000

13. TYPE OF REPORT
Annual Report

PERIOD COVERED (Inclusive dates)
Oct. 1, 1977 - Sept. 30, 1978

15. SUPPLEMENTARY NOTES

14. (Leave blank)

16. ABSTRACT (200 words or less)

During the period covered by this report, the expanding-aperture annular array system and an analysis of the focusing properties of an annular array were completed. Experiments were also undertaken to test the efficacy of spatial-temporal averaging to improve the signal-to-grain noise ratio in austenitic steel.

17. KEY WORDS AND DOCUMENT ANALYSIS

17a. DESCRIPTORS

17b. IDENTIFIERS/OPEN-ENDED TERMS

18. AVAILABILITY STATEMENT
Unlimited

19. SECURITY CLASS (This report): Unclassified

21. NO. OF PAGES

20. SECURITY CLASS (This page): Unclassified

22. PRICE
$

NRC FORM 335 (7-77)

UNITED STATES
NUCLEAR REGULATORY COMMISSION
WASHINGTON, D.C. 20555

OFFICIAL BUSINESS
PENALTY FOR PRIVATE USE, $300

POSTAGE AND FEES PAID
U.S. NUCLEAR REGULATORY
COMMISSION